Second-order nonlinear optical response of zigzag BN single-walled nanotubes

Vl. A. Margulis*
Department of Physics, Mordovian Ogarev State University, Saransk 430005, Russia

E. E. Muryumin and E. A. Gaiduk
Department of Chemistry, Mordovian Ogarev State University, Saransk 430005, Russia

(Received 24 June 2010; revised manuscript received 20 October 2010; published 14 December 2010)

A theory based on the two-band tight-binding approximation for π electrons is developed to describe the second-order nonlinear optical (NLO) properties of arrays of uniformly sized and well-aligned boron-nitride single-walled nanotubes (BN-SWNTs) with a zigzag achiral structure. It is assumed that the coherent light beam at frequency ω, incident upon the nanotube sample, is linearly polarized along the symmetry axis of the nanotubes. The long-axis NLO susceptibility $\chi^{(2)}(\omega)$ of those nanotubes is calculated within the independent nanotube approximation and in neglecting local-field effects. Using the perturbation-theory formalism in the crystal-momentum representation, we derive an explicit analytic expression for the $\chi^{(2)}(\omega)$ and apply it to study three distinct second-order NLO effects possible in the BN-SWNTs due to their noncentrosymmetric structure—namely, second-harmonic generation (SHG), linear electro-optical (LEO) effect, and nonlinear optical rectification (NOR). The theory is illustrated by numerical model calculations of the SHG, LEO, and NOR susceptibility spectra for several representative BN-SWNT ensembles consisting of large-diameter nanotubes. The calculated SHG spectra are found to be dominated by the highly peaked 2ω resonance at half the band-gap energy of the BN-SWNTs, where the absorption of light is negligible. Distinct features are also found in the LEO and NOR susceptibility spectra, e.g., a sudden switching of the susceptibility from a positive peak value to a negative peak one in the near vicinity of the fundamental absorption edge. A fairly large magnitude of those susceptibilities, reaching the order of 10^{-7} esu under off-resonant conditions and up to 10^{-6} esu in the resonant case, suggests that BN-SWNTs are a promising material for various electro-optical device applications.

DOI: 10.1103/PhysRevB.82.235426 PACS number(s): 78.67.Ch, 42.65.−k, 42.70.−a

I. INTRODUCTION

More than a decade after the original proposal[1,2] and the first successful synthesis,[3,4] boron-nitride nanotubes (BN-NTs) are still the subject of intensive theoretical and experimental research due to their remarkable physical properties (for a brief review of the subject, see Ref. 5). From a basic physics standpoint, perhaps the most significant feature of BN-NTs is that these nanotubes, unlike their carbon counterparts—carbon nanotubes,[6] are wide-band-gap semiconductors regardless of their diameter, helicity, or the number of the walls of the tube.[2] There are also many other features, such as, e.g., high thermal stability,[7] high resistivity to oxidation,[8] which make BN-NTs very attractive for practical applications in future nanoscale devices.

Recently, in a very interesting paper by Guo and Lin,[9] a systematic *ab initio* study of the second-order nonlinear optical (NLO) properties of BN-NTs within density-functional theory (DFT) has been carried out. From that study, it follows that BN-NTs have excellent perspectives to be used for NLO device applications, exhibiting fairly large second-order NLO coefficients $\chi^{(2)}_{\alpha\beta\gamma}$ (the Greek indices refer to the Cartesian coordinates x, y, and z) relevant to second-harmonic generation (SHG) and linear electron-optical (LEO) effect (the so-called Pockels effect). As far as we know, experiments on the measurement of those coefficients have not yet been conducted but are expected to be performed in the near future. Yet on the theoretical side, there also still remain some issues that have to be resolved in order to gain a detailed understanding of the second-order NLO properties of BN-NTs.

One of the most intriguing question that needs to be investigated is the following: what is the magnitude of the $\chi^{(2)}_{zzz}$ component of the second-order optical susceptibility tensor, which describes the NLO response of BN-NTs to the external electromagnetic field polarized along their axis (z axis)? The first-principles calculations, carried out by Guo and Lin,[9] answered this question, but not for all the nanotubes examined, showing, in particular, the vanishing of that component for the zigzag $(l,0)$ BN single-walled nanotubes (BN-SWNTs) if $l=5$, 9, and 27. From a point-symmetry-group analysis,[10] it follows, however, that the component $\chi^{(2)}_{zzz}$ should be nonzero for all the zigzag BN-SWNTs. Such a discrepancy between the group-theoretical analysis and the microscopic theory of Ref. 9 is puzzling, as was mentioned by the authors of Ref. 9 themselves. The zero value of the $\chi^{(2)}_{zzz}$ component, predicted in Ref. 9 for a number of the zigzag BN-SWNTs, looks very strange indeed, and it seems important therefore to try to clarify this point and to resolve the confusion.

Addressing this issue in the present paper, we adopt a fundamentally different approach than that used in Ref. 9. Namely, we concentrate here on the theoretical calculation of the $\chi^{(2)}_{zzz}$ for the zigzag BN-SWNTs within the framework of a simple model based on the two-band tight-binding (TB) approximation of their electronic structure.[11] To calculate $\chi^{(2)}_{zzz}$, we use a general perturbation-theory formalism developed by Genkin and Mednis[12] for the calculation of the NLO re-

sponse of bulk semiconductors in the independent-particle approximation. The advantage of the approach employed here is that it provides an explicit analytic expression for $\chi^{(2)}_{zzz}$, enabling numerical analysis of this quantity to be readily implemented for any nanotube considered. From such an analysis, carried out for those zigzag BN-SWNTs which have previously been predicted to have the vanishing component $\chi^{(2)}_{zzz}$,[9] it follows that there is nothing special with the $\chi^{(2)}_{zzz}$ in those nanotubes: the $\chi^{(2)}_{zzz}$ values are naturally nonzero, and the calculation shows what is the order of their magnitude.

Apart from being able to clarify the confusing picture that emerges from *ab initio* calculations by Guo and Lin,[9] our systematic analytical approach has the merit of elucidating the essential physics involved in the problem under discussion, providing much insight into the nature of the second-order optical nonlinearity of the BN-SWNTs. In particular, we find that the nonlinearity is associated with a combined effect of intraband and interband motion of π electrons in those nanotubes. That effect is shown to manifest itself in two physically distinct contributions to $\chi^{(2)}$, which originate from two different parts of the electron-position operator $\mathbf{r}$ and, hence, of the electric dipole moment $\mathbf{D}=-e\mathbf{r}$ of the π electrons in the crystal-momentum representation ($-e$ is the electron charge). The first part represents (up to a constant prefactor) the $\mathbf{k}$-space gradient operator $\nabla_{\mathbf{k}}$ ($\mathbf{k}$ is the electron wave vector) and, being diagonal in band index s, describes the effects relevant to purely intraband motion of the π electrons in band s. In contrast to this, the second part, which is expressed in terms of the transition matrix coupling a pair of electronic states with wave vector of $\mathbf{k}$, involves both intraband and interband effects. The intraband and interband contributions to the position operator $\mathbf{r}$ are "entangled" in second order in the external electric field intensity, leading to the expression for $\chi^{(2)}$ which can be written as the sum of two terms: the first term represents the contribution to $\chi^{(2)}$ associated with the change in proper dipole moment of Bloch electrons which occurs due to their interband motion, whereas the second term describes the contribution to $\chi^{(2)}$ originating from the $\mathbf{k}$-space variation in characteristics of the interband motion of the electrons in consequence of their intraband motion under the action of the external field and explicitly depending on the velocity of that variation through the $\mathbf{k}$-space gradient operator. Both the terms do not appear at all in the formulation of the second-order NLO response theory given in Ref. 13, which Guo and Lin have relied on in their paper.[9]

In the present paper, we also show the numerically calculated spectra of the susceptibility $\chi^{(2)}_{zzz}$, relevant to three second-order NLO effects in zigzag BN-SWNTs, namely, to the SHG process, the LEO effect and nonlinear optical rectification. The collection of the results we present here for several representative zigzag BN-SWNTs of fairly large diameters complements that obtained by Guo and Lin[9] from first principles and should turn out to be very useful as guidelines for future experimental studies.

The layout of the paper is as follows. In Sec. II, we present the principal ingredients of our theoretical analysis—the model and basic formalism. Our numerical results for the NLO susceptibility $\chi^{(2)}_{zzz}$ are reported and discussed in Sec. III. Finally, the conclusions are given in Sec. IV. The Appendix is devoted to a derivation of the general expression for the second-order NLO susceptibility within the Genkin-Mednis approach.

II. MODEL AND BASIC FORMALISM

The model system we consider represent an ensemble of very closely packed and well-aligned identical BN-SWNTs with a circular cross section of radius R, the surface density of the nanotubes in the plane perpendicular to their long axis being equal to $1/\pi R^2$. The nanotubes are assumed to be independent from each other and to have a zigzag achiral structure, which is characterized by the dual index $(l,0)$ in the standard notation.[6] As is known, BN-SWNTs, synthesized by means of different techniques,[14,15] exhibit a chirality preference in having just this structure. Note that, as far as we know, the system described above is not yet available experimentally but there is little doubt that, with the advance in technology, the fabrication of highly ordered arrays of identical BN-SWNTs will become possible (a step toward this goal has already been made by Wang *et al.*[16]). As to the electronic structure of such nanotubes, we treat it within a simple TB π-band model, neglecting the finite-tube-curvature effects. In favor of the model it should be noted that even its simplified $\mathbf{k}\cdot\mathbf{p}$ version has been successful enough in the linear optical response problem,[17] yielding the results in good agreement with experimental ones and requiring, at the same time, much less computation than more sophisticated many-body first-principles treatments. In view of this, we believe that it is justified to attempt to apply the present model to the description of the NLO response of the system under consideration, at least as a step toward an in-depth understanding and full treatment of the NLO properties of BN-SWNTs.

Because of depolarization effects in nanotubes,[18] a stronger NLO response is expected to occur for light polarized along the nanotube axis (z axis). For this reason, as well as for that pointed our above in Sec. I, in what follows we consider only the parallel polarization of an incident radiation with frequency components ω_1 and ω_2. Since only one component of the NLO susceptibility tensor $\chi^{(2)}_{\alpha\beta\gamma}(-\omega_\sigma=-\omega_1-\omega_2;\ \omega_1,\ \omega_2)$ is then relevant—namely, the long-axis component $\chi^{(2)}_{zzz}(-\omega_\sigma;\omega_1;\omega_2)$, further we drop the subscript z from the notation.

At first blush, the problem of the calculation of the susceptibility $\chi^{(2)}(-\omega_\sigma;\omega_1;\omega_2)$ may appear to be conceptually rather simple because there exists a standard quantum-mechanical formalism for such a calculation, elaborated in the pioneering works by Bloembergen *et al.*[19–21] and by Butcher and McLean.[22] In practice, however, the use of the general expression for the second-order NLO susceptibility tensor $\chi^{(2)}_{\alpha\beta\gamma}(-\omega_\sigma;\omega_1,\omega_2)$, obtained by those authors in terms of matrix elements of the electron momentum operator and electron-energy eigenvalues of a crystalline solid, is not a simple task since it requires knowledge of the momentum matrix elements among all the eigenstates of the crystal and summations over all its energy bands. In the case of the second-order nonlinear optics of semiconductors, which is of

primary interest for us here, the above-mentioned general expression for $\chi^{(2)}_{\alpha\beta\gamma}(-\omega_\sigma;\omega_1,\omega_2)$ can be simplified through the use of a three-band model, where only virtual electronic processes involving one valence and two conduction bands (vcc' processes) and virtual-hole processes involving one conduction and two valence bands ($vv'c$ processes) are assumed to contribute to $\chi^{(2)}_{\alpha\beta\gamma}$. Yet even within the framework of such a simplified model, the calculation of the susceptibility tensor $\chi^{(2)}_{\alpha\beta\gamma}(-\omega_\sigma;\omega_1,\omega_2)$ on the basis of the formalism of Refs. 19–22 is somewhat tricky because of the singular behavior of $\chi^{(2)}_{\alpha\beta\gamma}(-\omega_\sigma;\omega_1,\omega_2)$ when both ω_1 and ω_2 approach zero. The divergence of $\chi^{(2)}_{\alpha\beta\gamma}(-\omega_\sigma;\omega_1,\omega_2)$ in the zero-frequency limit has previously been discussed by Aspnes[23] and by Ghahramani *et al.*,[13] who have shown that the divergence is indeed only a fictitious one: once the expression for $\chi^{(2)}_{\alpha\beta\gamma}(-\omega_\sigma;\omega_1,\omega_2)$ is decomposed into divergent terms and a finite term, all the divergent terms vanish inasmuch as each of them involves a factor which has been proved to be equal to zero regardless of crystal symmetry class of the semiconductor providing the valence bands are completely filled whereas the conduction bands are empty. The corresponding proof, presented in Ref. 13 in the particular case of the SHG susceptibility tensor $\chi^{(2)}_{\alpha\beta\gamma}(-2\omega;\omega,\omega)$ is, however, far from being trivial, requiring, in particular, the derivation of a sum rule that allows one to isolate the intraband contributions to $\chi^{(2)}_{\alpha\beta\gamma}(-2\omega;\omega,\omega)$, which vanish for materials with filled valence bands.

To avoid such an inconvenience in the calculation of the susceptibility $\chi^{(2)}_{\alpha\beta\gamma}(-\omega_\sigma;\omega_1,\omega_2)$ in the general case of nondegenerate frequency mixing, it seems much easier and practical to use another approach which separates the intraband and interband motion of electrons from the very beginning and provides a well-behaved, general expression for $\chi^{(2)}_{\alpha\beta\gamma}(-\omega_\sigma;\omega_1,\omega_2)$ lacking the unphysical divergence at zero frequency. Such an approach was developed many years ago by Genkin and Mednis[12] in their theory of nonlinear conductivity of bulk semiconductors, and it is this approach that we shall rely on in the present paper. Note that a similar but slightly different formalism has later been developed by Sipe and Ghahramani,[24] who were able to show, again in the particular case of the SHG susceptibility tensor $\chi^{(2)}_{\alpha\beta\gamma}(-2\omega;\omega,\omega)$, that the expression for $\chi^{(2)}_{\alpha\beta\gamma}(-2\omega;\omega,\omega)$, which they have derived within the Genkin-Mednis-type perturbation scheme and which is free of any unphysical divergences at zero frequency, is equivalent to the expression for $\chi^{(2)}_{\alpha\beta\gamma}(-2\omega;\omega,\omega)$ obtained earlier,[13] by usual perturbation theory, for semiconductors with filled valence bands and empty conduction bands. As our intention in this paper is to consider not only SHG but also some other second-order NLO processes, we believe that the formulation of the NLO response theory on the basis of the Genkin-Mednis approach,[12] where no zero-frequency-limit problems exist at all, is more appropriate than the conventional one.[13]

The calculation method suggested in Ref. 12 is based on the perturbation-theory formalism in the crystal-momentum representation and is entirely within the framework of one-electron theory, neglecting exciton effects and local-field corrections. The validity of the theory for BN-SWNTs can certainly be disputed, but based on the recent *ab initio* DFT analysis of the linear optical response of those nanotubes, carried out without considering many-electron effects[25,26] as well as with taking them into account,[27,28] one can speculate on the adequacy of such a theory for studying the long-axis NLO susceptibility $\chi^{(2)}$, at least at a qualitative level. Indeed, it has been pointed out[25,26] that the local-field effects can be substantial only for the polarization of electromagnetic fields perpendicular to the tube axis. It has also been shown[27,28] that the net result of accounting for many-particle correlations is very minor indeed because of the almost complete cancellation of the contributions originating from the excitonic effects, on one hand, and from the quasiparticle self-energy corrections, on the other hand.

Following the prescription of Ref. 12 for the derivation of electronic contributions to the second-order NLO response of a clean, i.e., undoped, semiconductor in the electric dipole approximation, we find the two physically distinct ones, which have to be taken into account in the description of the NLO response of clean BN-SWNTs. As remarked earlier, the latter are wide-band-gap semiconductors in which the highest valence band (v band) is completely filled whereas the lowest conduction band (c band) is fully empty even at room temperature. In this case, the susceptibility $\chi^{(2)}$ can be partitioned as follows:

$$\chi^{(2)}(-\omega_\sigma;\omega_1,\omega_2)=\chi^{(2)}_{\mathrm{I}}(-\omega_\sigma;\omega_1,\omega_2)+\chi^{(2)}_{\mathrm{II}}(-\omega_\sigma;\omega_1,\omega_2). \tag{1}$$

Physically, both terms in the right-hand side of Eq. (1) are associated with a combined effect of intraband and interband motion of π electrons in the BN-SWNTs. However, those terms originate from different parts of the electron-position operator $\mathbf{r}$, which in the crystal momentum representation is given by[29,30]

$$\mathbf{r}=i\nabla_{\mathbf{k}}+i\mathbf{\Omega}, \tag{2}$$

where the first part, $i\nabla_{\mathbf{k}}$, being diagonal in both the band index s and the electron wave vector $\mathbf{k}$, describes the effects relevant to purely intraband motion of the π electrons, whereas the second part, the operator $i\mathbf{\Omega}$, involves both intraband and interband effects, being determined by its matrix elements which are diagonal only in $\mathbf{k}$

$$\mathbf{\Omega}_{ss'}(\mathbf{k})=\int U^*_{s\mathbf{k}}(\mathbf{r})\nabla_{\mathbf{k}}U_{s'\mathbf{k}}(\mathbf{r})d^3r. \tag{3}$$

Here $U_{s\mathbf{k}}(\mathbf{r})$ is the periodic modulation amplitude of the Bloch eigenfunction $\psi_{s\mathbf{k}}(\mathbf{r})=U_{s\mathbf{k}}(\mathbf{r})\exp(i\mathbf{kr})$. In developing a perturbation expansion within the framework of the Genkin-Mednis perturbation-theory scheme,[12] the two above-mentioned parts of the $\mathbf{r}$, "entangling" in the second order in the external field intensity, lead to the two physically distinct contributions to $\chi^{(2)}$, further referred to as the "shift" contribution ($\chi^{(2)}_{\mathrm{I}}$) and the "gradient" one ($\chi^{(2)}_{\mathrm{II}}$), which can be represented in the form (for the details of the derivation procedure, see the Appendix)

$$\chi^{(2)}_{\mathrm{I}}(-\omega_\sigma;\omega_1,\omega_2)=\frac{i\mathcal{N}e^3}{2\mathcal{V}\hbar^2}\sum_{\mathbf{k}}\sum_{P}\frac{\Omega_{vc}(\mathbf{k})[\Omega_{cc}(\mathbf{k})-\Omega_{vv}(\mathbf{k})]\Omega_{cv}(\mathbf{k})}{[\omega_{cv}(\mathbf{k})+\omega_1][\omega_{cv}(\mathbf{k})-\omega_2]}, \tag{4}$$

$$\chi_{\mathrm{II}}^{(2)}(-\omega_\sigma;\omega_1,\omega_2) = \frac{i\mathcal{N}e^3}{4\mathcal{V}\hbar^2}\sum_{\mathbf{k}}\sum_{P}\left\{\frac{\Omega_{vc}(\mathbf{k})}{\omega_{cv}(\mathbf{k})+\omega_1}\frac{\partial}{\partial k}\left[\frac{\Omega_{vc}(\mathbf{k})}{\omega_{cv}(\mathbf{k})-\omega_2}\right] - \frac{\Omega_{vc}(\mathbf{k})}{\omega_{cv}(\mathbf{k})-\omega_1}\frac{\partial}{\partial k}\left[\frac{\Omega_{vc}(\mathbf{k})}{\omega_{cv}(\mathbf{k})+\omega_2}\right]\right\}, \quad (5)$$

where $\mathcal{V}$ is a normalization volume of the system, $\mathcal{N}$ being the number of the nanotubes it contains, $\mathbf{k}$ is the π-electron wave vector with two components k_x and k_z, the former being quantized into the following discrete values:

$$k_x = \frac{m}{R} = \frac{2\pi m}{la_0}, \quad m = 0, \pm 1, \pm 2, \ldots, \pm(l-1), \quad (6)$$

due to the periodic boundary condition in the circumference direction of the zigzag $(l,0)$ BN-SWCNT under consideration whereas the latter (here and hereafter designated simply k) remains continuous for an infinitely long nanotube and takes values within the one-dimensional Brillouin zone $-k_{\mathrm{BZ}} \le k \le k_{\mathrm{BZ}}$ with $k_{\mathrm{BZ}} = \pi/a_0\sqrt{3}$ ($a_0 = 2.504$ Å is the lattice constant of the hexagonal BN). The other notations used is Eqs. (4) and (5) are as follows: Σ_P stands for the summation over all the different permutations of the frequencies ω_1, ω_2, and $-\omega_\sigma$, resulting in six terms, $\hbar\omega_{cv}(\mathbf{k}) = \varepsilon_{c\mathbf{k}} - \varepsilon_{v\mathbf{k}}$ is the energy distance between the two bands involved at fixed value of $\mathbf{k}$, and, finally, for brevity, we denote the z component of the vector matrix element $\mathbf{\Omega}_{ss'}(\mathbf{k})$ of Eq. (3) simply as $\Omega_{ss'}(\mathbf{k})$. The latter quantity [more precisely, $-e\Omega_{ss}(\mathbf{k})$] can be treated as a proper dipole moment of the electron in the Bloch state $|s\mathbf{k}\rangle$. As is well known,[30] an individual $\Omega_{ss}(\mathbf{k})$ is not uniquely defined because the Bloch amplitude $U_{s\mathbf{k}}$ can be multiplied by an arbitrary phase factor $\exp(i\theta_{s\mathbf{k}})$. However, the shift $\Omega_{cc}(\mathbf{k}) - \Omega_{vv}(\mathbf{k})$ is invariant under the gauge transformation $\exp(i\theta_{s\mathbf{k}})$ and is therefore a well-defined quantity[31,32] (in this connection, see also Ref. 33 and references therein).

Before we proceed further, note that the above formalism differs considerably from that used in Ref. 9, where the NLO response of BN-SWNTs was treated within a three-band model. It would not, therefore, be correct to claim that the two terms $\chi_{\mathrm{I}}^{(2)}$ and $\chi_{\mathrm{II}}^{(2)}$ in Eq. (1), which constitute the basis of our formulation of the NLO response theory, are lost or overlooked in the formulation given in Ref. 9: they cannot, indeed, appear there at all because they both are relevant only to the considered two-band model, in which the v- and c-band states themselves serve as intermediate states in the virtual electron transitions responsible for the second-order optical nonlinearities under discussion. In this context, we suspect that it is the difference in the initial models, adopted in the present paper on one hand and in Ref. 9 on the other hand, that mainly leads to discrepancies between the results reported here and those obtained in Ref. 9 (for details, see Sec. III further below). We cannot, however, definitely contend that this is just the case, since the full development of our approach, given in the Appendix, shows that two-band contributions to $\chi^{(2)}$ of the same type as in Eqs. (4) and (5) would appear necessarily, even if we adopted a three-band model. While we believe that the two-band approximation of the π-electronic structure of BN-SWNTs is sufficient to describe their second-order NLO response, there seem to be reasonable not to exclude *a priori* any of those models in a theoretical study of the response until experiment provides a clear indication on this subject. On the other hand, referring to the above-mentioned discrepancies, one cannot also exclude that there is something amiss either with the approach used in Ref. 9 or with its implementation so that further *ab initio* calculations of the $\chi^{(2)}$ would be highly desirable.

In order to find $\Omega_{ss'}(\mathbf{k})$, we use an analytic model of the π-electronic structure of the BN-SWNTs, developed in our previous paper[11] on the basis of the nearest-neighboring TB approximation and the zone-folding one. The latter is known to be a poor approximation for very thin nanotubes, such as, for example, (5,0) and (9,0) ones, but it seems to be reasonable enough for large-diameter nanotubes (with a diameter more than, say, 1.2–1.3 nm) because in this case the finite-tube-curvature effects, including σ-π hybridization, becomes negligibly small. Restricting our further consideration to just such thick nanotubes, we can write down the explicit expression for the π-electron-energy dispersion in a BN-SWNT $(l,0)$ as follows:[11]

$$\varepsilon_{s\mathbf{k}} = \varepsilon_{smk} = \pm\sqrt{\Delta^2 + t_0^2[1 + 4\nu_m^2 + 4\nu_m\cos(kd_0/2)]} \quad (7)$$

with

$$\nu_m = \cos(\pi m/l), \quad d_0 = \sqrt{3}a_0. \quad (8)$$

Here and hereafter, the upper (lower) sign refers to the $c(v)$ band, the azimuthal quantum number m, which is determined by Eq. (6), labels the size-quantized energy subbands of the v and c bands, t_0 is the transfer integral between π orbitals of nearest-neighboring B and N atoms, and Δ is the half difference of energies of π electrons localized on the sites occupied by those two atoms.

Within the framework of the considered model, which leaves out of account the finite-tube curvature effects, the Bloch modulation amplitudes $U_{c\mathbf{k}}(\mathbf{r})$ and $U_{v\mathbf{k}}(\mathbf{r})$ for the two bands involved can be approximately expressed in terms of the periodic parts $U_{\mathbf{K}}^{(1)}$ and $U_{\mathbf{K}}^{(2)}$ of the band-edge Bloch functions at the K point of the two-dimensional hexagonal Brillouin zone of the BN sheet as follows:

$$U_{s\mathbf{k}}(\mathbf{r}) = C_{s\mathbf{k}}^{(1)}U_{\mathbf{K}}^{(1)} + C_{s\mathbf{k}}^{(2)}U_{\mathbf{K}}^{(2)}, \quad (9)$$

where the superscripts 1 and 2 refer to the two sublattices occupied by B and N atoms, respectively, $\mathbf{K} = (2\pi/a)(1/3, 1/\sqrt{3})$ is the position vector of the K point, the coefficients $C_{s\mathbf{k}}^{(1)}$ and $C_{s\mathbf{k}}^{(2)}$ are the two components of the pseudospinor eigenstate that corresponds to the energy eigenvalue ε_{smk} of Eq. (7) and are given by

$$C_{s\mathbf{k}}^{(1)} = C_{smk}^{(1)} = -\frac{t_0}{\sqrt{2\varepsilon_{cmk}(\varepsilon_{cmk} \mp \Delta)}} \times [\exp(ikd_0/3) + 2\nu_m\exp(-ikd_0/3)], \quad (10)$$

$$C_{s\mathbf{k}}^{(2)} = C_{smk}^{(2)} = \pm \sqrt{\frac{\varepsilon_{cmk} \mp \Delta}{2\varepsilon_{cmk}}}. \tag{11}$$

In order to invoke the TB approximation, we express the periodic functions $U_{\mathbf{K}}^{(1)}(\mathbf{r})$ and $U_{\mathbf{K}}^{(2)}(\mathbf{r})$ entering Eq. (9) in terms of atomic $2p_z$ orbitals $\phi(\mathbf{r}-\mathbf{R}_n)$ as follows:

$$U_{\mathbf{K}}^{(1)}(\mathbf{r}) = \frac{1}{\sqrt{N}} \sum_{n=1}^{N} \phi(\mathbf{r}-\mathbf{R}_n)\exp[-i\mathbf{K}(\mathbf{r}-\mathbf{R}_n)], \tag{12}$$

$$U_{\mathbf{K}}^{(2)}(\mathbf{r}) = \frac{1}{\sqrt{N}} \sum_{n=1}^{N} \phi(\mathbf{r}-\mathbf{R}_n-\mathbf{d})\exp[-i\mathbf{K}(\mathbf{r}-\mathbf{R}_n-\mathbf{d})], \tag{13}$$

where $\mathbf{R}_n$ stands for the position vector of the nth primitive two-atomic unit cell of the unrolled BN-SWNT, $\mathbf{d}$ denotes the vector connecting the two atoms within the unit cell, and N is the total number of B and N sites, which is given by

$$N = 2\frac{2\pi RA}{\sqrt{3}a_0^2/2} = 4l\frac{A}{d_0}, \tag{14}$$

A being the normalized length of the nanotube.

Before we proceed further, it is worth mentioning that the zone-folding-derived π-electronic states of the zigzag BN-SWNT, presented above in Eq. (9), are double valley degenerate due to the presence of the states with exactly the same energy as that of Eq. (7) but associated with the valley centered at the K' point [with the position vector $\mathbf{K}' = (2\pi/a_0)(2/3,0)$] of the original two-dimensional Brillouin zone of the BN sheet. This valley degeneracy, as well as a double spin degeneracy of the states, will be taken into account further below in calculating the susceptibility $\chi^{(2)}$.

Using Eqs. (9)–(13) and taking into account that within the orthogonal TB scheme two localized atomic orbitals have zero overlap unless they are centered at the same site, we obtain the following expression for the interband matrix elements of Eq. (3):

$$\begin{aligned}\Omega_{cv}(\mathbf{k}) &= -\Omega_{vc}^{*}(\mathbf{k}) \\ &= \frac{d_0}{2}\frac{t_0^2}{\varepsilon_{cmk}\sqrt{\varepsilon_{cmk}^2-\Delta^2}} \times \left\{ \frac{\Delta}{\varepsilon_{cmk}}\nu_m \sin\left(\frac{kd_0}{2}\right) \right. \\ &\left. + \frac{i}{3}\left[1-2\nu_m^2+\nu_m\cos\left(\frac{kd_0}{2}\right)\right]\right\}\end{aligned} \tag{15}$$

whereas the diagonal elements of that equation are given by

$$\Omega_{ss}(\mathbf{k}) = i\frac{d_0}{6}\frac{t_0^2}{\varepsilon_{cmk}(\varepsilon_{cmk}\mp\Delta)} \times \left[1-2\nu_m^2+\nu_m\cos\left(\frac{kd_0}{2}\right)\right]. \tag{16}$$

For the present band-structure model, the sum over $\mathbf{k}$ in Eqs. (4) and (5) can be reduced to an integration over k and a sum over the subbands according to the prescription

$$\sum_{\mathbf{k}} \rightarrow \sum_{m=-(l-1)}^{l-1} 4\frac{A}{2\pi}\int_{-k_{\mathrm{BZ}}}^{k_{\mathrm{BZ}}} dk, \tag{17}$$

where the prefactor 4 originates from the above-mentioned spin and valley degeneracies. Then, after the introduction of dimensionless variables

$$u = \frac{k}{k_{BZ}}, \quad \mathcal{E}_{mu} = \frac{\varepsilon_{cmk}}{\Delta}, \quad \mathcal{Z}_i = \frac{\hbar\omega_i}{2\Delta} \quad (i=1,2) \tag{18}$$

and by inserting Eqs. (15) and (16) into Eq. (4), we further obtain the following expression for the "shift" contribution to $\chi^{(2)}$:

$$\begin{aligned}\chi_{\mathrm{I}}^{(2)}(-\omega_\sigma;\omega_1,\omega_2) = \frac{\pi}{2l^2}\frac{e^3}{\Delta^2}\left(\frac{t_0}{\Delta}\right)^6 \times \sum_{m=-(l-1)}^{l-1}\int_0^1 \mathcal{E}_{mu}^{-5}(\mathcal{E}_{mu}^2-1)^{-2} \\ \times [1-2\nu_m^2+\nu_m\cos(\pi u/2)] \\ \times \{\nu_m^2\sin^2(\pi u/2)+(\mathcal{E}_{mu}/3)^2 \times [1-2\nu_m^2 \\ +\nu_m\cos(\pi u/2)]^2\} \times \mathcal{P}(\mathcal{E}_{mu};\mathcal{Z}_1,\mathcal{Z}_2)du\end{aligned} \tag{19}$$

with

$$\mathcal{P}(\mathcal{E}_{mu};\mathcal{Z}_1,\mathcal{Z}_2) = \sum_P \frac{1}{(\mathcal{E}_{mu}+\mathcal{Z}_1)(\mathcal{E}_{mu}-\mathcal{Z}_2)}. \tag{20}$$

A similar calculation for the "gradient" contribution to $\chi^{(2)}$ [Eq. (5)] leads to

$$\begin{aligned}\chi_{\mathrm{II}}^{(2)}(-\omega_\sigma;\omega_1,\omega_2) = \frac{\pi}{2l^2}\frac{e^3}{\Delta^2}\left(\frac{t_0}{\Delta}\right)^6 \sum_{m=-(l-1)}^{l-1}\nu_m\int_0^1 \mathcal{E}_{mu}^{-5}(\mathcal{E}_{mu}^2-1)^{-1} \\ \times \{[1-2\nu_m^2+\nu_m\cos(\pi u/2)] \\ \times [\nu_m\sin^2(\pi u/2)+(1/2)(\Delta/t_0)^2 \\ \times \mathcal{E}_{mu}^2\cos(\pi u/2)]+(1/2)(\Delta/t_0)^2 \\ \times \nu_m\mathcal{E}_{mu}^2\sin^2(\pi u/2)\} \\ \times \mathcal{P}(\mathcal{E}_{mu};\mathcal{Z}_1,\mathcal{Z}_2)du.\end{aligned} \tag{21}$$

The explicit expressions, obtained above for the two independent contributions to $\chi^{(2)}$, represent the main analytical result of the paper. In the general case, their sum, given by Eq. (1), determines the second-order NLO susceptibility $\chi^{(2)}(-\omega_\sigma;\omega_1,\omega_2)$ describing the so-called three-photon mixing process whose net result is the generation of radiation at the sum frequency $\omega_\sigma=\omega_1+\omega_2$ in the presence of two pump laser beams at frequencies ω_1 and ω_2. In the particular case in which only a laser beam of one frequency ω is present, the susceptibility $\chi^{(2)}(-2\omega;\omega,\omega)$ is responsible for the SHG of light, and will be denoted here as $\chi_{\mathrm{SHG}}^{(2)}(\omega)$.

Another specific three-photon mixing process may occur when one coherent light wave at frequency ω is incident on a BN-SWNT sample which is subjected to a dc electric field. The latter can be considered as a coherent superposition of photons of zero frequency. In the above-mentioned process, one dc "photon" and single ac photon mixes up with the result that an additional polarization and absorption appears

at frequency ω. Both these effects (LEO and electroabsorption) are described by the susceptibility $\chi^{(2)}(-\omega;0,\omega)$, the former being determined by its real part whereas the latter by its imaginary part. For the sake of notation convenience, those parts will be denoted here as $\chi^{(2)}_{\mathrm{LEO}}(\omega)$ and $\chi^{(2)}_{\mathrm{EA}}(\omega)$, respectively.

The susceptibility $\chi^{(2)}(-\omega;0,\omega)$ is relevant to one more second-order NLO effect, namely, the nonlinear optical rectification (NOR), that is, the generation of a dc electric field by an optical beam of frequency ω. Indeed, in agreement with the permutaion symmetry requirement,[20,34,35] the corresponding NOR susceptibility $\chi^{(2)}_{\mathrm{NOR}}(0;\omega,-\omega)=\chi^{(2)}_{\mathrm{LEO}}(\omega)$ when the frequency ω lies in the transparent region of the material. In this region, $\chi^{(2)}_{\mathrm{LEO}}(\omega)$ is connected with the so-called Pockels coefficient $r_{\mathrm{P}}(\omega)$ by the relation (in the esu units we are using in the paper)

$$\chi^{(2)}_{\mathrm{LEO}}(\omega) = -\frac{1}{8\pi} n^4(\omega) r_{\mathrm{P}}(\omega), \tag{22}$$

where $n(\omega)$ is the linear real index of refraction,

$$n(\omega) = \sqrt{1 + 4\pi\,\mathrm{Re}\,\chi^{(1)}(\omega)} \tag{23}$$

with $\chi^{(1)}(\omega)$ being the linear optical susceptibility.

In what follows, we confine ourselves to the particular frequency combinations indicated above, which are of significant interest from the point of view of possible device applications. The general case of nondegenerate three-photon mixing in BN-SWNTs, resulting in the sum (or difference)-frequency generation, will be considered in detail elsewhere.[36]

In order to obtain physically corrected results for the susceptibility $\chi^{(2)}$, one should also regularize the singularities inherent in Eqs. (4) and (5) under resonant conditions. It can be done in the usual manner, namely, by adding an imaginary part to the energy of exited states, which describes their decay due to electron collisions. For computational purposes, this is essentially equivalent to the replacement of $\mathcal{E}_{mu}$ by $\mathcal{E}_{mu}+i\Gamma$ in Eq. (20), where Γ represents an inverse excited-state lifetime expressed in units of $2\Delta/\hbar$. Applying a partial fraction expansion to single out the individual resonant denominators in Eq. (20) and separating the real and imaginary parts of $\mathcal{P}$ in that equation, we then find

$$\begin{aligned}\mathrm{Re}\,\mathcal{P}(\mathcal{E}_{mu};\mathcal{Z},\mathcal{Z}) &= -\mathcal{E}_{mu}^{-1}\{[(\mathcal{E}_{mu}-\mathcal{Z})\mathcal{D}(\mathcal{E}_{mu}-\mathcal{Z},\Gamma) - 4(\mathcal{E}_{mu}-2\mathcal{Z}) \\ &\quad\times\mathcal{D}(\mathcal{E}_{mu}-2\mathcal{Z},\Gamma)] + [\mathcal{Z}\to-\mathcal{Z}]\},\end{aligned} \tag{24}$$

$$\begin{aligned}\mathrm{Im}\,\mathcal{P}(\mathcal{E}_{mu};\mathcal{Z},\mathcal{Z}) &= \Gamma\mathcal{E}_{mu}^{-1}\{[\mathcal{D}(\mathcal{E}_{mu}-\mathcal{Z},\Gamma) - 4\mathcal{D}(\mathcal{E}_{mu}-2\mathcal{Z}),\Gamma] + [\mathcal{Z}\to-\mathcal{Z}]\}\end{aligned} \tag{25}$$

in the case of the SHG process whereas in the case of both the LEO effect and the NOR one, we obtain

$$\begin{aligned}\mathrm{Re}\,\mathcal{P}(\mathcal{E}_{mu};0,\mathcal{Z}) &= \{[2\mathcal{E}_{mu}^{-1}(\mathcal{E}_{mu}-\mathcal{Z})\mathcal{D}(\mathcal{E}_{mu}-\mathcal{Z},\Gamma) + [(\mathcal{E}_{mu}-\mathcal{Z})^2-\Gamma^2] \\ &\quad\times\mathcal{D}^2(\mathcal{E}_{mu}-\mathcal{Z},\Gamma)\} + \{\mathcal{Z}\to-\mathcal{Z}\},\end{aligned} \tag{26}$$

$$\begin{aligned}\mathrm{Im}\,\mathcal{P}(\mathcal{E}_{mu};0,\mathcal{Z}) &= -2\Gamma\{[\mathcal{E}_{mu}^{-1}\mathcal{D}(\mathcal{E}_{mu}-\mathcal{Z},\Gamma) + (\mathcal{E}_{mu}-\mathcal{Z}) \\ &\quad\times\mathcal{D}^2(\mathcal{E}_{mu}-\mathcal{Z},\Gamma)] + [\mathcal{Z}\to-\mathcal{Z}]\},\end{aligned} \tag{27}$$

where we have adopted the following shorthand notation:

$$\mathcal{D}(\mathcal{E}_{mu}-\mathcal{Z},\Gamma) = \frac{1}{(\mathcal{E}_{mu}-\mathcal{Z})^2+\Gamma^2}. \tag{28}$$

In the context of the present calculation of $\chi^{(2)}$, it is interesting to evaluate the quantity

$$\delta_M(\omega_\sigma) = \frac{\chi^{(2)}(-\omega_\sigma;\omega_1,\omega_2)}{\chi^{(1)}(\omega_\sigma)\chi^{(1)}(\omega_1)\chi^{(1)}(\omega_2)} \tag{29}$$

and to assess the validity of the so-called Miller phenomenological rule[37] in the case of the well-ordered tubular structures under discussion. According to Miller's original proposal,[37] the quantity $\delta_M(\omega)$ is expected to be a slowly varying function of ω, and, what is more, $\delta_M(0)$ should be a certain universal constant for a wide range of noncentrasymmetric inorganic materials. To test the latter conjecture, a comparative analysis would be necessary of linear and second-order NLO properties of a number of inorganic tubular forms of III-V compounds, available at present, such as, e.g., BN,[3–5] AlN,[38] and GaN.[39] Such an analysis is certainly beyond the scope of the present paper. The only thing we can do here is to examine the frequency variation in δ_M for the BN-SWNTs under consideration. To this end, we further calculate their linear optical susceptibility $\chi^{(1)}(\omega)$ within the same TB π band-structure model we have used above.

We start with the Genkin-Mednis dispersion formula for $\chi^{(1)}(\omega)$,[12] which can be written in the form

$$\begin{aligned}\chi^{(1)}(\omega) = \frac{\mathcal{N}e^2}{\mathcal{V}\hbar}\sum_{\mathbf{k}}|\Omega_{cv}(\mathbf{k})|^2\Bigg[&\frac{1}{\omega_{cv}(\mathbf{k})-\omega-i\gamma} \\ &+\frac{1}{\omega_{cv}(\mathbf{k})+\omega+i\gamma}\Bigg],\end{aligned} \tag{30}$$

where γ is the phenomenological broadening parameter regularizing the resonant divergencies, which is assumed to be independent of $\mathbf{k}$. Note that the above expression for $\chi^{(1)}(\omega)$ has already been exploited to study the linear optical properties of the zigzag BN-SWNTs.[17] However, that study was based on the Král-Mele-Tománek $\mathbf{k}\cdot\mathbf{p}$ band-structure model of such nanotubes,[31] rather than on the TB model we use here. Substituting Eq. (15) into Eq. (30) and using Eqs. (17) and (18), we obtain, after separating Eq. (30) into real and imaginary parts,

$$\chi^{(1)}(\omega) = \mathrm{Re}\,\chi^{(1)}(\omega) + i\,\mathrm{Im}\,\chi^{(1)}(\omega), \tag{31}$$

$$\left.\begin{matrix}\mathrm{Re}\,\chi^{(1)}(\omega)\\ \mathrm{Im}\,\chi^{(1)}(\omega)\end{matrix}\right\} = \frac{6\pi}{l^2}\left(\frac{e^2/d_0}{\Delta}\right)\left(\frac{t_0}{\Delta}\right)^4 \sum_{m=-(l-1)}^{l-1} \times \int_0^1 du \mathcal{E}_{mu}^{-4}(\mathcal{E}_{mu}^2-1)^{-1} \times \{\nu_m^2 \sin^2(\pi u/2) + (\mathcal{E}_{mu}/3)^2 \times [1-2\nu_m^2+\nu_m \cos(\pi u/2)]^2\} \times \begin{cases}\mathrm{Re}\,Q(\mathcal{E}_{mu},\mathcal{Z})\\ \mathrm{Im}\,Q(\mathcal{E}_{mu},\mathcal{Z})\end{cases}, \tag{32}$$

where

$$\mathrm{Re}\,Q(\mathcal{E}_{mu},\mathcal{Z}) = [(\mathcal{E}_{mu}-\mathcal{Z})D(\mathcal{E}_{mu}-\mathcal{Z}),\Gamma] + [\mathcal{Z}\rightarrow -\mathcal{Z}], \tag{33}$$

$$\mathrm{Im}\,Q(\mathcal{E}_{mu},\mathcal{Z}) = -\Gamma[D(\mathcal{E}_{mu}-\mathcal{Z},\Gamma) + D(\mathcal{E}_{mu}+\mathcal{Z},\Gamma)]. \tag{34}$$

Equations (19), (21), and (32), which constitute our final expressions for the first- and the second-order optical response of the BN-SWNTs, respectively, can no longer be simplified because neither the integration over u nor the summation over m in those equations may be performed analytically. However, the rather cumbersome-looking results of the above-mentioned equations lend themselves readily to numerical analysis, which will be carried out in Sec. III for several representative zigzag BN-SWNTs.

III. NUMERICAL RESULTS AND DISCUSSION

As a paradigm for the second-order NLO properties to be expected for uniform ensembles of the zigzag BN-SWNTs, we present here the numerical results following from Eqs. (19) and (21) for four such ensembles consisting, respectively, of the nanotubes (17,0), (21,0), (25,0), and (27,0). Note that for the first three above-mentioned structures the first-principles calculations by Guo and Lin[9] yielded nonzero $\chi^{(2)}_{zzz}$ values whereas the vanishing of that component has been reported in the same paper for the BN-SWNT (27,0). Also, the zero value of $\chi^{(2)}_{zzz}$ has been predicted in Ref. 9 for the BN-SWNTs (5,0) and (9,0), which will be not considered in the present paper because our theory, as mentioned above, is limited in its applicability to the BN-SWNTs of fairly large diameters.

In the calculations discussed below we have used the following values for the parameters entering our model: t_0 =2.4 eV, Δ=2.2 eV, and Γ=0.01. Note that the above values are exactly the same as those used in our previous paper,[17] where they were chosen to get the best fit to the experimental optical absorption spectrum measured by Lauret *et al.*[40] on assembly of large-diameter BN-SWNTs. It should be stressed, however, that the specific predictions we make below regarding the spectral behavior of $\chi^{(2)}$ are not very sensitive to those values of the model parameters.

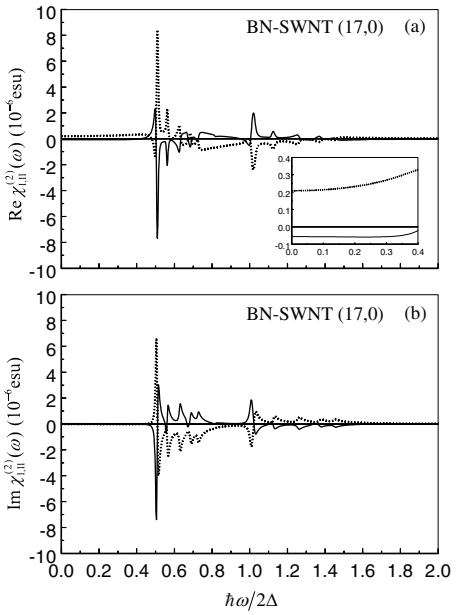

FIG. 1. The real and imaginary parts [panels (a) and (b), respectively] of two contributions $\chi^{(2)}_{\mathrm{I}}(\omega)$ and $\chi^{(2)}_{\mathrm{II}}(\omega)$ to the total SHG susceptibility $\chi^{(2)}_{\mathrm{SHG}}(\omega)$ calculated for a uniform ensemble of the zigzag BN-SWNTs (17,0). Solid lines represent the results obtained for the "shift" contribution $\chi^{(2)}_{\mathrm{I}}(\omega)$ using Eqs. (19), (24), and (25). Dotted lines show the results obtained for the "gradient" contribution $\chi^{(2)}_{\mathrm{II}}(\omega)$ using Eq. (21), (24), and (25). Both the contributions are plotted as functions of the normalized photon energy $\hbar\omega/2\Delta$. In panel (a), the inset shows the variation in both the Re $\chi^{(2)}_{\mathrm{I}}(\omega)$ and Re $\chi^{(2)}_{\mathrm{II}}(\omega)$ below half the band-gap energy of the nanotubes. Notice the opposite signs of those contributions and the fact that the absolute value of $\chi^{(2)}_{\mathrm{II}}(0)$ is larger than that of $\chi^{(2)}_{\mathrm{I}}(0)$, which implies a positive value of the total $\chi^{(2)}_{\mathrm{SHG}}(0)$ (cf. Table II in Ref. 9).

A. Second-harmonic generation

We start our numerical study by considering the susceptibility $\chi^{(2)}_{\mathrm{SHG}}$ responsible for the SHG of light. In Sec. II, we have shown that there are two independent contributions to $\chi^{(2)}$, specified by Eqs. (19) and (21), respectively. It is therefore of interest to investigate their relative weight in the second-order NLO processed under discussion. To this end, in Fig. 1, we display the spectral dependences of the real [Fig. 1(a)] and imaginary [Fig. 1(b)] parts of both the contributions $\chi^{(2)}_{\mathrm{I}}(-2\omega;\omega,\omega)$ and $\chi^{(2)}_{\mathrm{II}}(-2\omega;\omega,\omega)$ to the SHG susceptibility $\chi^{(2)}_{\mathrm{SHG}}(\omega)$, calculated for the uniform ensemble of the BN-SWNTs (17,0). As is see from Fig. 1, both the contributions should be considered as being equally significant in calculating the total $\chi^{(2)}_{\mathrm{SHG}}(\omega)$. Moreover, since the curves of the real as well as the imaginary part of $\chi^{(2)}_{\mathrm{I}}(-2\omega;\omega,\omega)$ and $\chi^{(2)}_{\mathrm{II}}(-2\omega;\omega,\omega)$ in Fig. 1 look like nearly mirror images of each other relative to a zero line of $\chi^{(2)}_{\mathrm{I,II}}$, it is the subtle balance of the contributions that determines the resulting magnitude of the $\chi^{(2)}_{\mathrm{SHG}}(\omega)$.

In Fig. 2, we display the real and imaginary parts of the total susceptibility $\chi^{(2)}_{\mathrm{SHG}}(\omega)$, derived by summing up the two curves in Fig. 1(a) and those in Fig. 1(b), respectively. The results for the absolute value of the SHG susceptibility $|\chi^{(2)}_{\mathrm{SHG}}(\omega)|$ are plotted in the same figure.

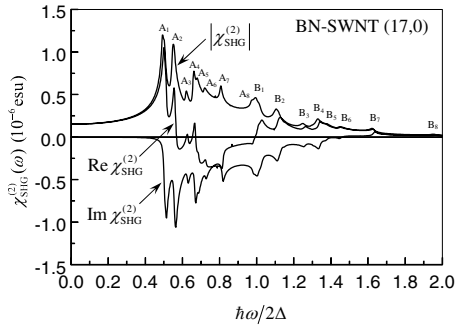

FIG. 2. The SHG susceptibility $\chi^{(2)}_{SHG}(\omega)$ for a uniform ensemble of the BN-SWNTs (17,0). The real part, imaginary part, and absolute magnitude of the $\chi^{(2)}_{SHG}(\omega)$ are plotted versus the dimensionless photon energy $\hbar\omega/2\Delta$. The capital alphabetic letters A_i and B_i ($i=1,2,\ldots,8$) on the top of the peaks correspond to our labeling convention for the spectral features originating from the 2ω and ω resonant terms of Eqs. (24) and (25) (for details, see the text).

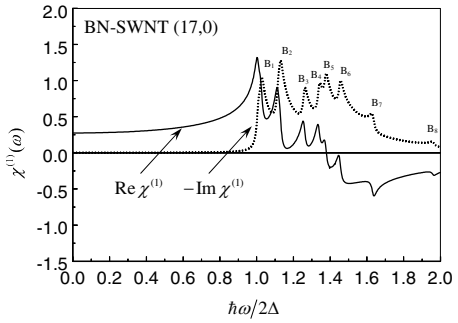

FIG. 3. Spectra of the real and imaginary parts (solid line and dotted one, respectively) of the linear optical susceptibility $\chi^{(1)}(\omega)$ calculated for a uniform ensemble of the BN-SWNTs (17,0) using Eq. (32). Symbols from B_1 to B_8 on the top of the peaks in the spectrum of the imaginary part of $\chi^{(1)}(\omega)$ correspond to our labeling convention for direct one-photon resonant transitions between the valence- and conduction-energy subbands with the same index m (for details, see the text).

The calculated spectrum of the $|\chi^{(2)}_{SHG}(\omega)|$, shown in Fig. 2, exhibits pronounced resonant peak structures originating from both single- and double-frequency resonant terms of Eqs. (24) and (25). Examining the contributions of those terms to the SHG spectrum, we find that the spectral features observed in the photon energy range $\hbar\omega/2\Delta<1$ (in Fig. 2, they are labeled with symbols $A_1, A_2, \ldots, A_8$ in order of increasing photon energy) are entirely due to the 2ω resonant terms of Eqs. (24) and (25). In contrast, only relatively small contributions of those terms to the $|\chi^{(2)}_{SHG}|$ spectrum are found at higher photon energies so that it is the single-frequency (ω) resonant term of Eqs. (24) and (25) that dominate the spectral behavior of the $|\chi^{(2)}_{SHG}(\omega)|$ in the range $\hbar\omega/2\Delta\geq 1$ (in Fig. 2, the corresponding features in the $|\chi^{(2)}_{SHG}|$ spectrum are labeled with symbols from B_1 to B_8 in going from lower to higher energies).

The above conclusions are supported by a direct comparison of the $|\chi^{(2)}_{SHG}|$ spectrum with the linear optical absorption one calculated for the BN-SWNT (17,0) using Eq. (32). The values of both the real and imaginary parts of the linear optical susceptibility $\chi^{(1)}(\omega)$ are shown in Fig. 3 versus the dimensionless photon energy $\hbar\omega/2\Delta$. As is clearly seen from that figure, the spectrum of Im $\chi^{(1)}(\omega)$, which corresponds to the optical absorption one, is featureless below the threshold value $\hbar\omega/2\Delta=1$. In the region above the threshold, however, the spectrum exhibits the pronounced characteristic features labeled $B_1, B_2, \ldots, B_8$ in Fig. 3. Using the π-electronic band-structure diagram of the BN-SWNT (17,0), shown in Fig. 4, we can attribute these features to direct optical transitions between successive pairs of the valence- and conduction-π-electron-energy subbands with the same azimuthal quantum number m, which are mirror symmetrically situated with respect to the Fermi level $E_F=0$. Being proportional to the joint density of (electronic) states (JDOS), the probability of such transitions (hereafter referred to as $v_m \rightarrow c_m$ transitions) is extremely large just near the energy-subband edges at $k=0$, where van Hove's singularities of the JDOS are located. However, not all the dipole-allowed resonant interband transitions produce well-resolved individual peaks in the Im $\chi^{(1)}(\omega)$ spectrum shown in Fig. 3. The reason for this is that some of the nearest-neighboring energy subbands in the π-electronic spectrum of the BN-SWNTs are almost degenerate near the $k=0$ point. If the energy spacing between them (say, between the subbands with indices m and $m+1$) is smaller than the broadening energy parameter $\hbar\gamma$, then the peaks corresponding to $v_m \rightarrow c_m$ and $v_{m+1} \rightarrow c_{m+1}$ transitions will tend to merge, forming, as a result, a single peak of a larger width. Turning now to the BN-SWNT (17,0) under consideration, we find that this is the case for $v_{11} \rightarrow c_{11}$ and $v_{12} \rightarrow c_{12}$ transitions, which produce the first peak in the Im $\chi^{(1)}(\omega)$ spectrum, labeled B_1 in Fig. 3. The same is the case for the second peak (B_2) in that spectrum, which may be ascribed to both $v_{10} \rightarrow c_{10}$ and $v_{13} \rightarrow c_{13}$ transitions.

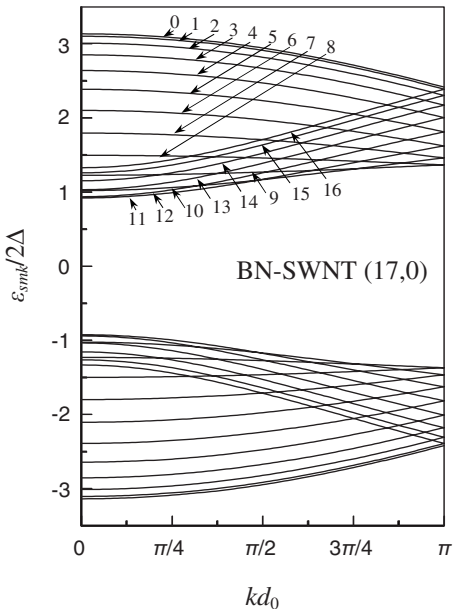

FIG. 4. π-electronic band-structure diagram of the BN-SWNT (17,0), as obtained within the TB framework [Eq. (7)]. Arrows indicate the one-dimensional energy subbands ε_{smk} of the c band, specified by the azimuthal quantum number m ranging from 0 to 16 for the present nanotube (Ref. 41).

The other spectral features (from B_3 to B_8) observed in Fig. 3 arise (in sequential order) from the following interband transitions: $v_{14} \rightarrow c_{14}$, $v_9 \rightarrow c_9$, $v_{15} \rightarrow c_{15}$, $v_{16} \rightarrow c_{16}$, $v_8 \rightarrow c_8$, and $v_7 \rightarrow c_7$. These transitions are well separated in their energy due to fairly large (as compared to $\hbar\gamma$) energy spacing (around $k=0$) between the corresponding nearest-neighboring subbands in the v and c bands (Fig. 4).

Comparing our graphs for $|\chi^{(2)}_{\mathrm{SHG}}(\omega)|$ and Im $\chi^{(1)}(\omega)$, given in Figs. 2 and 3, respectively, shows that the energy positions of the peaks, marked with the same labels $B_i (i=1,2,\ldots,8)$ in both the spectra are identical. This corroborates the conclusion, we have drawn above that the $|\chi^{(2)}_{\mathrm{SHG}}(\omega)|$ spectrum can naturally be divided into two parts, namely, the low-energy part ($\hbar\omega/2\Delta < 1$), which is clearly dominated by several highly peaked 2ω resonances, and the higher-energy part ($\hbar\omega/2\Delta \geq 1$) consisting of a few distinct ω resonance peaks with much smaller amplitudes. The latter feature is not surprising since each 2ω resonance is weighted by a factor of four as compared to the corresponding ω resonance [see Eqs. (24) and (25)].

It is also worthwhile to note that the SHG intensity $|\chi^{(2)}_{\mathrm{SHG}}(\omega)|$ reaches its absolute maximum (peak A_1) of about 1.2×10^{-6} esu when the photon energy $\hbar\omega$ is near one half the fundamental band-gap energy Δ_g is the π-electron spectrum of the nanotube at $k=0$, the Δ_g being well approximated by 2Δ. Indeed, according to Eq. (7), Δ_g can be written as

$$\Delta_g = 2\Delta \sqrt{1 + \left(\frac{t_0}{\Delta}\right)^2 (1 + 2\nu_{m_g})^2}, \tag{35}$$

where the integer m_g is the azimuthal quantum number referring to the highest valence and lowest conduction subbands in the band structure of the BN-SWNT $(l,0)$,

$$m_g = \begin{cases} \dfrac{2l}{3} & \text{if } l = 3M \\ \left[\dfrac{2l}{3} + 1\right] & \text{if } l = 3M+1 \\ \left[\dfrac{2l}{3}\right] & \text{if } l = 3M+2 \end{cases} \tag{36}$$

with integer M. Here the square brackets stand for the integral part of the number they contain. For the values of the model parameters, which we have used in our calculations, and for the possible values of m_g, which correspond to large-diameter $(l,0)$ BN-SWNTs (with a diameter more than 1.2–1.3 nm), the second term under the square root sign in Eq. (35) is negligibly small as compared to unit so that 2Δ will be a good approximation to Δ_g for all such nanotubes.[42]

The above-mentioned peak value of the SHG intensity in the near-half-band-gap region ($\hbar\omega \approx \Delta_g/2$) is almost one order of magnitude larger than that predicted theoretically for bulk BN crystals.[43] We attribute this enhancement to the quasi-one-dimensional (1D) nature of the π-electronic states in BN-SWNTs, which makes conditions for three peculiarities of their electronic structure to occur at one and the same point of the nanotube 1D Brillouin zone, namely, at the Γ point ($k=0$). Those peculiarities are the maximum absolute value of the dipole interband transition matrix element, the minimum value of the width of the fundamental band gap, and the theoretical infinite JDOS associated with van Hove's singularities. Note that essentially the same underlying physics is responsible for the very large third-order optical nonlinearity of semiconducting single-walled carbon nanotubes,[44] which has recently been observed experimentally.[45]

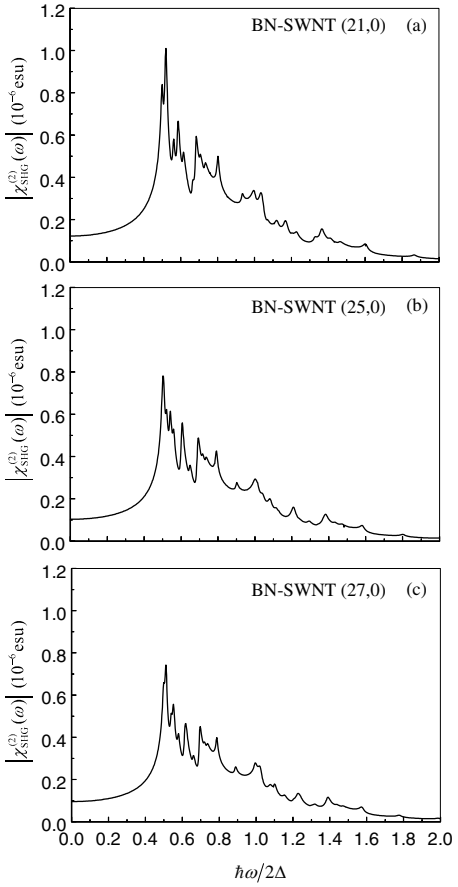

FIG. 5. SHG spectra for three uniform BN-SWNT ensembles consisting, respectively, of the nanotubes with chirality indices (a) (21,0), (b) (25,0), and (c) (27,0). The latter ones are indicated in the upper part of the panels. The calculated $|\chi^{(2)}_{\mathrm{SHG}}(\omega)|$ values are plotted versus the normalized photon energy $\hbar\omega/2\Delta$.

In order to demonstrate the effect of the main geometrical parameter of the nanotubes—namely, their diameter, on the amplitude $|\chi^{(2)}_{\mathrm{SHG}}(\omega)|$ of the SHG signal, we have calculated the absolute values of the SHG susceptibility for the three other uniform ensembles of the zigzag BN-SWNTs, which have been chosen for our investigation. The results of the calculation are shown in Figs. 5(a)–5(c) for the ensembles consisting, respectively, of the BN-SWNTs with indices (21,0), (25,0), and (27,0).

Several general conclusions can be drawn from the spectra presented in Fig. 5. First, for the thicker nanotubes, there are more resonant peaks in the SHG spectra—the fact which directly reflects the larger number of the size-quantized energy subbands in the π-band structure of those nanotubes. Second, an overall reduction in the SHG intensity with increasing l (i.e., with an increase in the radius R of the nanotubes in an ensemble) is clearly seen at all photon energies,

TABLE I. Calculated static SHG susceptibility $\chi^{(2)}_{\mathrm{SHG}}(0)$ and LEO coefficient $r_{\mathrm{P}}(0)$ (both in units of 10^{-6} esu) for four uniform BN-SWNT ensembles consisting, respectively, of the zigzag nanotubes with chirality indices (17,0), (21,0), (25,0), and (27,0). Results from *ab initio* calculations by Guo and Lin (Ref. 9) are also shown for comparison in the same units.

BN-SWNT	$\chi^{(2)}_{\mathrm{SHG}}(0)$	$\chi^{(2)}_{\mathrm{SHG}}(0)$ [a]	$r_{\mathrm{P}}(0)$	$r_{\mathrm{P}}(0)$ [a]
(17,0)	0.152	−1.197	−0.169	0.106
(21,0)	0.123	−1.149	−0.137	0.102
(25,0)	0.104	−1.095	−0.115	0.099
(27,0)	0.096	0.0	−0.107	0.0

[a]Reference 9.

including the off-resonance region $\hbar\omega/2\Delta<1/2$ as well as the resonance one $\hbar\omega/2\Delta\geq 1/2$. The above trend in $|\chi^{(2)}_{\mathrm{SHG}}(\omega)|$ to be smaller in magnitude for thicker nanotubes is consistent with the recent similar observation made by Guo and Lin[9] on the basis of their *ab initio* DFT calculations. Third, each of the SHG spectra is seen to be dominated by the most prominent 2ω resonant peak located at the pump photon energy of about one half the band-gap energy Δ_g. Since the BN-SWNTs are almost transparent in the near-half-band-gap region (cf. Fig. 3), the SHG signal, which is given by the square of $|\chi^{(2)}_{\mathrm{SHG}}(\omega)|$, can be greatly enhanced without any optical losses if $\hbar\omega$ is fine tuned to Δ. This suggests that the well-order arrays of the BN-SWNTs considered are of significant interest from the point of view of practical SHG applications.

As has already been mentioned, the SHG susceptibility of the BN-SWNTs under discussion has recently been calculated by Guo and Lin[9] using a first-principles method. However, no results for SHG spectra of those nanotubes have been presented in Ref. 9, and only static $\chi^{(2)}_{\mathrm{SHG}}(0)$ values of the SHG susceptibility have been reported therein (see Table II in that reference). This prevents any conclusive comparison of our theoretical calculation of the SHG susceptibility $\chi^{(2)}_{\mathrm{SHG}}(\omega)$ with the *ab initio* study of the $\chi^{(2)}_{\mathrm{SHG}}$ performed in Ref. 9. Still, a comparison of the corresponding zero-frequency results for the SHG susceptibility is quite possible, and it shows important differences between them (see Table I). First, the $\chi^{(2)}_{\mathrm{SHG}}(0)$ values for the BN-SWNTs (17,0), (21,0), and (25,0) are about one order of magnitude smaller than the corresponding values reported in Ref. 9. Second, the BN-SWNTs display positive $\chi^{(2)}_{\mathrm{SHG}}(0)$ values, which correspond to the second-order optical nonlinearity that includes the positive $\chi^{(2)}_{\mathrm{II}}(0)$ contribution dominating the negative $\chi^{(2)}_{\mathrm{I}}(0)$ one, as demonstrated in Fig. 1(a). In contrast, the first-principles calculations carried out by Guo and Lin[9] predict negative values of the long-axis component $\chi^{(2)}_{zzz}$ of the zero-frequency SHG susceptibility tensor. The last but not the least contradiction between our zero-frequency results for the SHG susceptibility and those presented in Ref. 9 concern the BN-SWNT (27,0). For that nanotube, as follows from Fig. 5(c), $\chi^{(2)}_{\mathrm{SHG}}(0)$ has a finite value (as one should expect), which is in sharp contrast with the vanishing $\chi^{(2)}_{\mathrm{SHG}}(0)$ value obtained in Ref. 9.

The above-mentioned large disparity between our calculated results for $\chi^{(2)}_{\mathrm{SHG}}(0)$ and those of Guo and Lin[9] clearly indicated the necessity of a systematic experimental investigation of the SHG susceptibility of the BN-SWNTs both at low frequency and over a wide frequency range. It this connection, one comment is in order. As remarked earlier, most experimental BN-SWNT samples available at present contain a mixture of the nanotubes differing by their diameters and possibly chiralities. Therefore, in real experimental conditions, only an average SHG signal from a great number of the nanotubes can be measured. As a result of averaging, many individual resonances (especially those with small amplitudes) seen in the SHG spectra in Figs. 2 and 5 may turn out to be smeared out so that only the most prominent 2ω and ω resonant structures occurring in those spectra can be expected to be observed for ensembles containing many different BN-SWNTs.

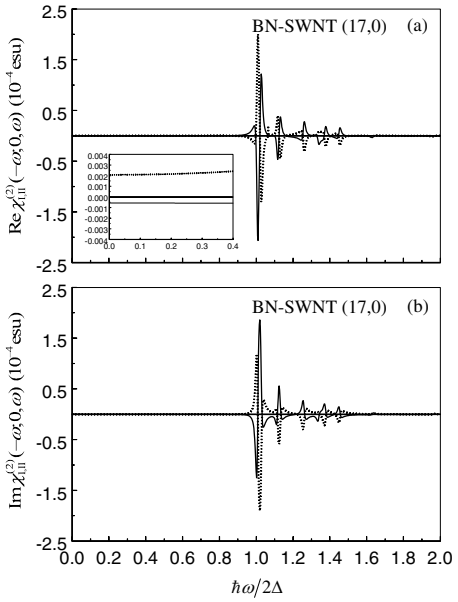

FIG. 6. The real and imaginary parts [panels (a) and (b), respectively] of two contributions $\chi^{(2)}_{\mathrm{I}}(\omega)$ and $\chi^{(2)}_{\mathrm{II}}(\omega)$ to the susceptibility $\chi^{(2)}(-\omega;0,\omega)$ calculated for a uniform ensemble of the zigzag BN-SWNTs (17,0). Solid lines represent the results obtained for the "shift" contribution $\chi^{(2)}_{\mathrm{I}}(\omega)$ using Eqs. (19), (26), and (27). Dotted lines show the results obtained for the "gradient" contribution $\chi^{(2)}_{\mathrm{II}}(\omega)$ using Eq. (21), (26), and (27). Both the contributions are plotted as functions of the normalized photon energy $\hbar\omega/2\Delta$. In panel (a), the inset shows the variation in both the Re $\chi^{(2)}_{\mathrm{I}}(\omega)$ and Re $\chi^{(2)}_{\mathrm{II}}(\omega)$ below half the band-gap energy of the nanotubes.

B. Pockels effect and nonlinear optical rectification

We now present the results of our numerical calculations of the susceptibility $\chi^{(2)}(-\omega;0,\omega)$ responsible for the LEO effect, electroabsorption (EA) and NOR. All the effects are important for possible optoelectronic applications of BN-NTs, e.g., optical switching.

As the expression for $\chi^{(2)}$ [Eq. (1)] contains two terms $\chi^{(2)}_{\mathrm{I}}$ and $\chi^{(2)}_{\mathrm{II}}$, we start our survey of the results with Fig. 6, where the spectra of the two distinct contributions to $\chi^{(2)}(-\omega;0,\omega)$ are shown for both the LEO effect [Fig. 6(a)]

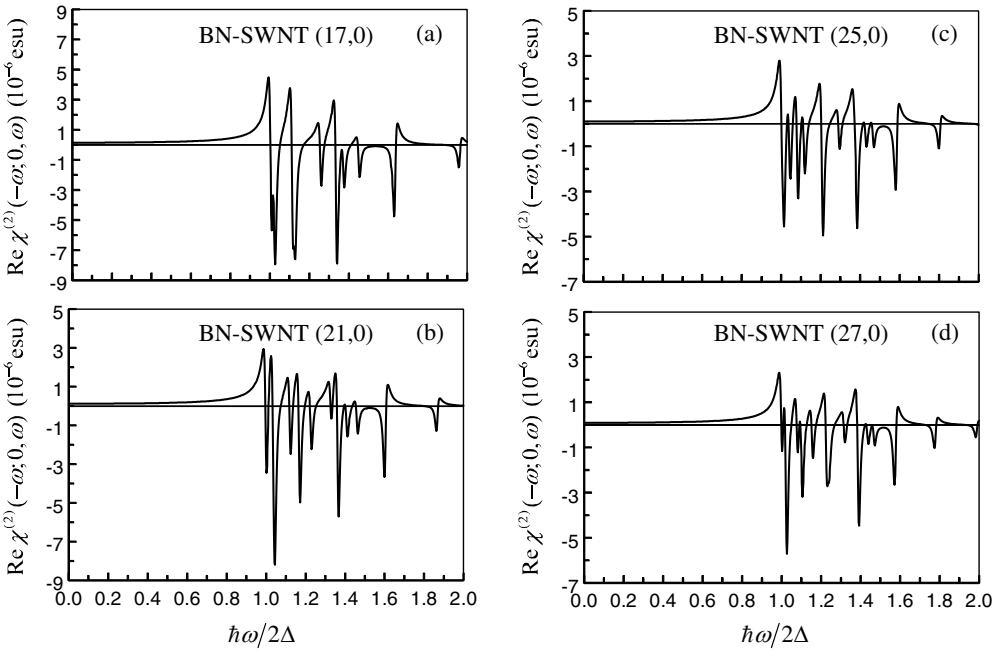

FIG. 7. Spectra of the real part of the susceptibility $\chi^{(2)}(-\omega;0,\omega)$ calculated for four uniform BN-SWNT ensembles consisting, respectively, of the nanotubes with chirality indices (a) (17,0), (b) (21,0), (c) (25,0), and (d) (27,0). The latter ones are indicated in the upper part of the panels. The calculated values of the Re $\chi^{(2)}(-\omega;0,\omega)$ are plotted versus the normalized photon energy $\hbar\omega/2\Delta$.

and the EA one [Fig. 6(b)] in the case of a uniform ensemble of the BN-SWNTs (17,0). Again, similarly to the SHG case (Fig. 1), those two contributions to $\chi^{(2)}$ are comparable in magnitude over the whole frequency range considered, as is clearly illustrated by the graphs in Fig. 6, and, hence, they both have to be taken into account in developing a proper theoretical treatment of the second-order NLO properties of BN-SWNTs. Moreover, that figure gives a clear indication as to which of the two is predominant in the zero-frequency limit ($\omega\rightarrow 0$) [see the inset in Fig. 6(a)]. Evidently, the positive $\chi^{(2)}_{\mathrm{II}}(0)$ contribution prevails in the total LEO susceptibility $\chi^{(2)}_{\mathrm{LEO}}(0)$, thus providing a positive sign for the latter and, hence, a negative sign for the corresponding zero-frequency Pockels coefficient $r_{\mathrm{P}}(0)$ [see Eq. (22)]. This is in accord with our above finding of $\chi^{(2)}_{\mathrm{SHG}}(0)$ having a positive sign, since the total SHG and LEO susceptibilities, being but two special cases of the general second-order nonlinearity, are equal at $\omega=0$. We can again note that the signs of the $\chi^{(2)}_{\mathrm{LEO}}(0)$ and $r_{\mathrm{P}}(0)$ are opposite to those predicted by Guo and Lin[9] (see Table I).

In Fig. 6, for all the BN-SWNT ensembles considered, we show the calculated spectra of the LEO susceptibility $\chi^{(2)}_{\mathrm{LEO}}(\omega)=\mathrm{Re}\ \chi^{(2)}(-\omega;0,\omega)$. In view of the relation between the LEO and NOR susceptibilities, mentioned in Sec. II, the same figure presents our results for the NOR effect as well. The latter is conventionally detected as an electric bias signal appearing at the electrode terminals of a sample under the action of a light beam incident on the sample.[46–48] In the case of a sample consisting of monosized and aligned BN-SWNTs of length A, which we are interested in here, the optical rectification voltage V_0 is given by

$$V_0=\frac{4\pi}{n_0^2}P^{(2)}(0)A, \tag{37}$$

where $P^{(2)}(0)$ is the static electronic polarization of the sample, induced by the incident light beam of intensity I_ω, propagating in the direction perpendicular to the symmetry axis of the nanotubes,

$$P^{(2)}(0)=\frac{8\pi}{cn_0}\chi^{(2)}_{\mathrm{NOR}}(0;\omega,-\omega)I_\omega \tag{38}$$

with c being the speed of light in free space. Thus, using the above equations and the data from Fig. 7, we can estimate the magnitude of the bias for the uniform BN-SWNT ensembles under consideration (see further below).

Referring to Fig. 7, it also tells us how a dc electric field $\mathbf{E}_0$ directed parallel to the BN-SWNT symmetry axis changes the optical refractive index of the well-ordered arrays of such nanotubes. Since the π-electronic band structure of the nanotubes is unaffected by the applied longitudinal electric field, the above-mentioned refractive index charge $\Delta n(\omega)$, occurring in the first order in E_0, can be expressed as follows:

$$\Delta n(\omega)=\frac{2\pi}{n_0}\chi^{(2)}_{\mathrm{LEO}}(\omega)E_0. \tag{39}$$

The change in the refractive index results in the phase shift $\Delta\Phi$ of the light wave passing through the sample, which is given by

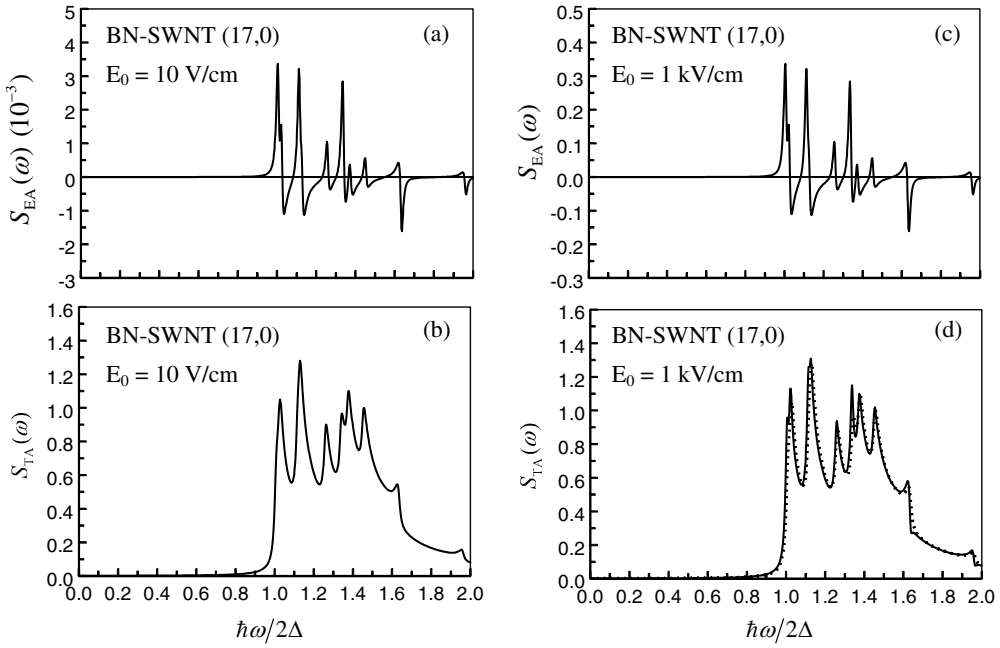

FIG. 8. The electroabsorption spectra $S_{EA}(\omega)$ [panels (a) and (c)] and the total absorption spectra $S_{TA}(\omega)$ [panels (b) and (d)] calculated for a uniform ensemble of the BN-SWNTs (17,0) using Eqs. (42) and (41), respectively. The value of the electric field strength E_0 is chosen to be 10 V/cm (upper panels) and 1 kV/cm (bottom panels). In panel (d), the linear absorption spectrum $S_{LA}(\omega)$ (dotted line) is shown for comparison. The only difference between the $S_{EA}(\omega)$ curves, shown in the upper panels, is the intensity of the resonant peaks, which are just scaled up when E_0 increases. In the $S_{TA}(\omega)$ spectra, plotted in the bottom panels, we see no significant change either of the shape of the resonant peaks or of their intensity as a function of E_0.

$$\Delta\Phi = \frac{\omega}{c} l_{op} \Delta n(\omega), \tag{40}$$

where l_{op} is the optical path length. Such a shift caused by the LEO effect should be easily detected experimentally by employing the two-beam interference method,[49] where the first light beam is incident on the BN-SWNT sample, whereas the second one has passed through the sample. Allowing measurements of very small refractive index changes, that method, even though it requires a coherent light source, affords the opportunity to determine the Pockels coefficient using only one light beam propagating in the electro-optical material. This is also of practical interest from the viewpoint of possible applications of BN-SWNTs themselves in phase-shifted devices. An order-of-magnitude estimation of $\Delta n(\omega)$ and $\Delta\Phi$ will be given further below for the BN-SWNT ensembles under consideration.

Returning to Fig. 7, it is worthwhile to note an important common feature inherent in all the spectra shown in that figure. Namely, in the near vicinity of the fundamental absorption edge, the LEO (or NOR) susceptibility changes drastically from a positive peak value to a negative peak one, passing through zero exactly at $\hbar\omega/2\Delta = 1$. As can be seen in Fig. 7, such a sudden switching of the susceptibility from maximum positive values to maximum negative ones and vice versa occurs repeatedly as we move away from the absorption edge to higher photon energies. This implies that one can adjust the radiation frequency ω so that its slight variation will "switch on" or "switch off" the optical rectification voltage V_0 at the terminals of the BN-SWNT sample. In the same manner, one can produce drastic changes in the optical refractive index $n(\omega)$ of the sample subjected to a dc electric field E_0 [see Eq. (39)]. We believe that both the above-mentioned effects are potentially very important for the future development of BN-SWNT-based NLO devices, even though their practical implementation does not seem to be a simple task. The point is that the increase in the nonlinearity, which occurs as $\hbar\omega$ approaches 2Δ (Fig. 7), is accompanied by an equivalent increase in optical losses. This can clearly be observed in Fig. 3, where the magnitude of the linear absorption (LA) signal $S_{LA}(\omega) = -\mathrm{Im}\ \chi^{(1)}(\omega)$ of the ensemble of the BN-SWNTs (17,0) has been plotted as a function of $\hbar\omega/2\Delta$. Figure 8 illustrates the situation occurring in the presence of a dc electric field E_0 applied to those nanotubes along their symmetry axis. In this case, to take full account of absorption, one has to consider two contribution to the total absorption (TA) signal $S_{TA}(\omega)$

$$S_{TA}(\omega) = S_{LA}(\omega) + S_{EA}(\omega), \tag{41}$$

where $S_{EA}(\omega)$ is the magnitude of the EA signal,

$$S_{EA}(\omega) = -\chi^{(2)}_{EA}(\omega) E_0 = -\mathrm{Im}\ \chi^{(2)}(-\omega; 0, \omega) E_0. \tag{42}$$

Using the above equations, we have calculated both the EA and TA spectra of the ensemble of the BN-SWNTs (17,0) for two different values of the electric field strength: $E_0 = 10$ V/cm and $E_0 = 1$ kV/cm.[50] The results of the calculations are displayed in Fig. 8.

Comparing Figs. 3 and 8 indicates that the absorption spectrum changes very little, even if a rather strong electric field of 1 kV/cm is applied to the nanotubes. This implies

that it will at least be extremely hard, if not impossible, to decouple large refractive index changes, produced by a variation in the radiation frequency, from the undesirable absorption losses for photons with energy greater than the band-gap energy. However, as is seen from Figs. 7 and 8, the ratio $\chi^{(2)}_{\mathrm{LEO}}/S_{\mathrm{TA}}$ can be improved drastically in the spectral region lying well below the fundamental absorption edge. The plots in Fig. 7 show that the magnitude of $\chi^{(2)}_{\mathrm{LEO}}$ is on the order of 10^{-7} esu in the nonresonant situation. According to Refs. 9 and 17, the linear refractive index n_0 is about 2 for the BN-SWNTs under consideration. Using the above values of $\chi^{(2)}_{\mathrm{LEO}}$ and n_0 in Eq. (39), and assuming an applied dc electric field E_0 of 1 kV/cm, we get $\Delta n \approx 0.01$. In the 1.30–1.55 μm optical telecommunication wavelength range, such a change in $n(\omega)$ is sufficient to introduce a $\pi/4$ phase shift [see Eq. (40)] in a less-than-10 μm-length dielectric waveguide structure, where a uniform array of well-aligned BN-SWNTs, fabricated in the form of a thin film, can be used as the core of the structure. This suggests that those nanotubes are a prospective material for the designs of novel nano-optoelectronic devices in the area of integrated optics and optical communication systems.

In this context, it is also of interest to estimate the magnitude of the NOR effect in the BN-SWNTs. Combining Eqs. (37) and (38) and using the calculated off-resonance $\chi^{(2)}_{\mathrm{NOR}}$ of 10^{-7} esu, we deduce an optical rectification voltage V_0 of about 5 μV in the case of an array of the BN-SWNTs, 1 μm in length, irradiated by laser pulses with a power density of ~ 100 kW/cm^2. Based on this estimate, we can conclude that BN-SWNTs may be an appropriate material for future uses in high-intensity-optical-pulse detectors, successfully competing with compositionally asymmetric GaAs/AlGaAs multiple quantum-well structures in which the magnitude of V_0 achieves the value of 250 nV under the continuous illumination by a CO_2 10.6 μm laser with a power density of 60 W/cm^2.[51]

Finally, we briefly comment on our theoretical results for the Miller coefficient δ_{M} [Eq. (29)]. As we are concerned with two different second-order NLO susceptibilities $\chi^{(2)}_{\mathrm{SHG}}$ and $\chi^{(2)}_{\mathrm{LEO}}$, the corresponding Miller coefficients $\delta^{\mathrm{SHG}}_{\mathrm{M}}(\omega)$ and $\delta^{\mathrm{LEO}}_{\mathrm{M}}(\omega)$ need to be considered separately. It should be noticed that Miller's $\delta_{\mathrm{M}}(\omega_\sigma)$, as given by Eq. (29), has physical meaning only in the range where all $\hbar\omega$'s are well below the band-gap energy Δ_g. Since absorption is not significant in that region, we can write the $\delta^{\mathrm{SHG}}_{\mathrm{M}}(\omega)$ as

$$\delta^{\mathrm{SHG}}_{\mathrm{M}}(\omega) = \frac{\mathrm{Re}\ \chi^{(2)}_{\mathrm{SHG}}(\omega)}{\mathrm{Re}\ \chi^{(1)}(2\omega)[\mathrm{Re}\ \chi^{(1)}(\omega)]^2} \tag{43}$$

whereas the $\delta^{\mathrm{LEO}}_{\mathrm{M}}(\omega)$ can be expressed as

$$\delta^{\mathrm{LEO}}_{\mathrm{M}}(\omega) = \frac{\chi^{(2)}_{\mathrm{LEO}}(\omega)}{\chi^{(1)}(0)[\mathrm{Re}\ \chi^{(1)}(\omega)]^2}. \tag{44}$$

In Fig. 9, both the functions, $\delta^{\mathrm{SHG}}_{\mathrm{M}}(\omega)$ and $\delta^{\mathrm{LEO}}_{\mathrm{M}}(\omega)$, are plotted versus $\hbar\omega/2\Delta$ at photon energies below half the band-gap energy of the BN-SWNTs under study. As one can see from that figure, for each of the BN-SWNT ensemble considered, $\delta^{\mathrm{SHG}}_{\mathrm{M}}(0)$ coincides with $\delta^{\mathrm{LEO}}_{\mathrm{M}}(0)$ due to the equivalence of the SHG and LEO susceptibilities at zero frequency, a result we have commented on earlier in this paper. However, neither the $\delta^{\mathrm{SHG}}_{\mathrm{M}}(0)$ nor the $\delta^{\mathrm{LEO}}_{\mathrm{M}}(0)$ is an universal constant: their magnitudes are different for the ensembles consisting of the nanotubes with different chirality indices. Besides, Fig. 9 predicts both the $\delta^{\mathrm{SHG}}_{\mathrm{M}}(\omega)$ and $\delta^{\mathrm{LEO}}_{\mathrm{M}}(\omega)$ to be a slightly decreasing function of ω over the photon energy range plotted in that figure. This implies that Miller's empirical rule[37] is not fulfilled even for one and the same class of the nanotubes, namely, the zigzag BN-SWNTs $(l,0)$. As remarked earlier, it would be most desirable to have this rule tested for a wider range of nanotube materials with a similar noncentrosymmetric structure, which are available at present.[38,39]

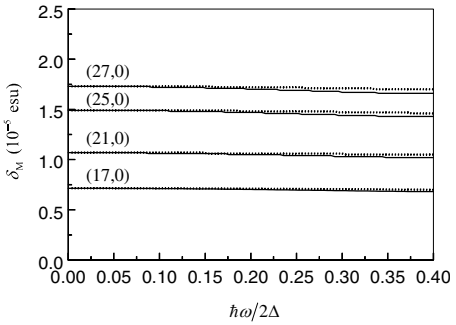

FIG. 9. Frequency dispersion of Miller's coefficients $\delta^{\mathrm{SHG}}_{\mathrm{M}}(\omega)$ (solid lines) and $\delta^{\mathrm{LEO}}_{\mathrm{M}}(\omega)$ (dotted lines) calculated for four uniform BN-SWNT ensembles consisting, respectively, of the nanotubes with chirality indices (17,0), (21,0), (25,0), and (27,0). The latter ones are indicated in the left part of the panel where the lines make their start.

IV. CONCLUSIONS

To summarize, in this paper we have presented a theory that describes the second-order NLO response of arrays of uniformly sized and well-aligned zigzag BN-SWNTs of fairly large diameters. Unlike the previous theoretical study of the problem,[9] based on a first-principles DFT method, we have used here quite a different approach, originally proposed by Genkin and Mednis[12] for the calculation of the NLO response of bulk semiconductors in the independent-particle approximation. The advantage of the approach is that it properly takes into account the combined effect of intraband and interband motion of π electrons in the BN-SWNTs, thereby enabling a clear physical picture of the optical nonlinearity to be drawn.

Relying on this approach and using a simple TB model for the π-electronic band structure of the BN-SWNTs, developed in our previous paper,[11] we have derived an explicit analytic expression for the second-order NLO susceptibility $\chi^{(2)}(\omega)$ of the uniform BN-SWNT arrays, which includes two contributions associated with the above-mentioned combined effect: the "shift" contribution [Eq. (19)] and the "gradient" one [Eq. (21)], both are comparable in magnitude over the whole photon-energy range considered. We have revealed that it is the "gradient" contribution that prevails in the susceptibility $\chi^{(2)}(\omega)$ at zero frequency, yielding positive $\chi^{(2)}(0)$ values for the considered nanotubes. Our finding of $\chi^{(2)}(0)$

being positive is in sharp contrast with negative $\chi^{(2)}(0)$ values predicted for the same nanotubes in Ref. 9, which seem highly counterintuitive, at least at the present level of understanding. We have also shown that there is nothing sensational with those zigzag BN-SWNTs $(l,0)$ for which a previous *ab initio* study[9] yielded a zero value of the $\chi^{(2)}(0)$: indeed, they all display nonzero $\chi^{(2)}(0)$ values while in this paper we have presented those values only for the nanotubes of sufficiently large diameters.

An important outcome of our theory is the prediction of distinct resonant features, which should be observable in the SHG, LEO, and NOR susceptibility spectra of the considered BN-SWNT ensembles. For example, in all the calculated SHG spectra, we have found multiple 2ω and ω resonant structures, the most intense peak being always just at half the band-gap energy of the nanotubes, where optical losses are negligible. Another interesting result to notice is that the LEO (or NOR) susceptibility changes drastically from a positive peak value to a negative peak one, passing through zero exactly at the fundamental absorption edge. Such a switching effect is likely to be very important for the future development of BN-SWNT-based electro-optical devices.

In conclusion, we would like to stress that our primary motivation in this paper has been to provide a coherent picture of second-order optical nonlinearities in the BN-SWNTs at the simplest level of approximation. We believe that the model used here is sufficient to grasp the relevant basic physics so that the results obtained should serve as useful guides for future more refined theoretical studies. However, a more fundamental need is for some experimental data in order to test our findings. We hope that such studies will reveal most clearly the potential utility of BN-SWNTs as a new material for NLO applications.

ACKNOWLEDGMENTS

This research was supported by the Russian Foundation for Basic Research through Grant No. 08-02-01035-a.

APPENDIX: DERIVATION OF THE $\chi^{(2)}$ EXPRESSION WITHIN THE GENKIN-MEDNIS PERTURBATION SCHEME

Since the formulation of the second-order NLO response theory, which we have relied on in the present paper, could be used as an alternative also for other applications, we present here the detailed derivation of Eqs. (4) and (5) of the text, closely following a procedure proposed by Genkin and Mednis.[12]

We start with the standard Hamiltonian H for an electron of mass m_0, moving in a periodic lattice potential $V(\mathbf{r})$ and interacting with the electric field $\mathbf{E}(t)$ of the incident electromagnetic wave. In the electric dipole approximation, the Hamiltonian is given by

$$H = \frac{1}{2m_0}\left[\mathbf{p} + \frac{e}{c}\mathbf{A}(t)\right]^2 + V(\mathbf{r}), \tag{A1}$$

where the vector potential $\mathbf{A}(t)$ of the external field $\mathbf{E}(t) = (-1/c)(\partial\mathbf{A}/\partial t)$ is only dependent on time t and independent of $\mathbf{r}$. A state of the electron then evolves in time according to Schrödinger's equation

$$i\hbar\frac{\partial}{\partial t}\Psi(\mathbf{r},t) = H\Psi(\mathbf{r},t), \tag{A2}$$

where the wave function $\Psi(\mathbf{r},t)$ can be expressed linearly in terms of a complete orthonormal set of the Bloch wave functions

$$\psi_{s\boldsymbol{\kappa}}(\mathbf{r}) = U_{s\boldsymbol{\kappa}}(\mathbf{r})\exp(i\boldsymbol{\kappa}\mathbf{r}) \tag{A3}$$

with shifted wave vector

$$\boldsymbol{\kappa} = \mathbf{k} + \frac{e}{\hbar c}\mathbf{A}(t), \tag{A4}$$

that is,

$$\Psi(\mathbf{r},t) = \sum_{s,\mathbf{k}} a_{s\mathbf{k}}(t)\psi_{s\boldsymbol{\kappa}}(\mathbf{r}). \tag{A5}$$

Using Eqs. (A2)–(A5), we find, in the usual way, the equation for the expansion coefficients $a_{s\mathbf{k}}(t)$,

$$i\hbar\frac{\partial}{\partial t}a_{s\mathbf{k}}(t) = \sum_{s'}[\varepsilon_{s\boldsymbol{\kappa}}\delta_{ss'} + ie\boldsymbol{\Omega}_{ss'}(\boldsymbol{\kappa})\cdot\mathbf{E}(t)]a_{s'\mathbf{k}}(t), \tag{A6}$$

where $\delta_{ss'}$ is the Kronecker symbol, $\varepsilon_{s\boldsymbol{\kappa}}$ is the energy eigenvalue corresponding to the Bloch eigenfunction $\psi_{s\boldsymbol{\kappa}}(\mathbf{r})$, and $\boldsymbol{\Omega}_{ss'}(\boldsymbol{\kappa})$ is given by Eq. (3) of the text with $\mathbf{k}$ replaced by $\boldsymbol{\kappa}$. The second term in the square brackets on the right-hand side of Eq. (A6) has a clear physical meaning. At $s'=s$, that term describes the variation in the energy of the electron as it moves within its original band s under the action of the applied field $\mathbf{E}(t)$. At $s'\neq s$, the same term describes the interband motion of the electron as driven by the field.

To proceed further, it is convenient to write down Eq. (A6) in symbolic operator notation

$$i\hbar\frac{\partial}{\partial t}|a_{\mathbf{k}}(t)\rangle = \hat{\mathcal{H}}(\boldsymbol{\kappa},t)|a_{\mathbf{k}}(t)\rangle, \tag{A7}$$

$$\hat{\mathcal{H}}(\boldsymbol{\kappa},t) = \hat{\mathcal{H}}_0(\boldsymbol{\kappa}) + \hat{\mathcal{H}}_1(\boldsymbol{\kappa},t), \tag{A8}$$

treating the coefficients $a_{s\mathbf{k}}(t)$ as the components of a vector $|a_{\mathbf{k}}(t)\rangle$ in the "band-index space" where operators $\hat{\mathcal{H}}_0(\boldsymbol{\kappa})$ and $\hat{\mathcal{H}}_1(\boldsymbol{\kappa},t)$ are defined as the operators whose matrix elements are given, respectively, by the first and the second terms in the square brackets in Eq. (A6). As is seen from that equation, the operator $\hat{\mathcal{H}}_0(\boldsymbol{\kappa})$ is already represented by the diagonal matrix $\varepsilon_{s\boldsymbol{\kappa}}\delta_{ss'}$. To diagonalize the operator $\hat{\mathcal{H}}(\boldsymbol{\kappa},t)$ as a whole, we shall carry out a unitary transformation $\hat{O}(\boldsymbol{\kappa},t)$ from the original $a_{s\mathbf{k}}(t)$'s to the new coefficients $c_{s\mathbf{k}}(t)$,

$$a_{s\mathbf{k}}(t) = \sum_{s'} O_{ss'}(\boldsymbol{\kappa},t)c_{s'\mathbf{k}}(t) \tag{A9}$$

so that the evolution of the latter in time should be governed by an effective Hamiltonian $\hat{\mathcal{H}}^{\text{eff}}(\boldsymbol{\kappa},t)$, which is diagonal in s, i.e.,

$$\mathcal{H}^{\text{eff}}_{ss'}(\boldsymbol{\kappa},t)=0 \quad \text{for } s\neq s', \tag{A10}$$

and hence

$$i\hbar\frac{\partial}{\partial t}c_{s\mathbf{k}}(t)=\mathcal{H}^{\text{eff}}_{ss}(\boldsymbol{\kappa},t)c_{s\mathbf{k}}(t). \tag{A11}$$

Using Eqs. (A4), (A7), and (A9), it is not hard to write down the Hamiltonian $\hat{\mathcal{H}}^{\text{eff}}(\boldsymbol{\kappa},t)$ in terms of the unitary operator $\hat{O}(\boldsymbol{\kappa},t)$

$$\hat{\mathcal{H}}^{\text{eff}}(\boldsymbol{\kappa},t)=\hat{O}^{\dagger}(\boldsymbol{\kappa},t)[\hat{\mathcal{H}}_0(\boldsymbol{\kappa})+\hat{\mathcal{H}}_1(\boldsymbol{\kappa},t)]\hat{O}(\boldsymbol{\kappa},t) + ie\hat{O}^{\dagger}(\boldsymbol{\kappa},t)\nabla_{\boldsymbol{\kappa}}\hat{O}(\boldsymbol{\kappa},t)\mathbf{E}(t)-i\hbar\hat{O}^{\dagger}(\boldsymbol{\kappa},t)\frac{\partial}{\partial t}\hat{O}(\boldsymbol{\kappa},t). \tag{A12}$$

The hard part of the problem at hand is solving Eq. (A10) with a view to finding the nondiagonal matrix elements $O_{ss'}(\boldsymbol{\kappa},t)$; the diagonal ones are determined by the additional condition $O_{ss}(\boldsymbol{\kappa},t)=O^{\dagger}_{ss}(\boldsymbol{\kappa},t)$. Once explicit expressions for those matrix elements are obtained, the electric dipole polarization $\mathbf{P}(t)$—the macroscopic source of NLO response of the electronic system—can be found by calculating the expectation value of the dipole moment operator $\mathbf{D}=-e\mathbf{r}=-ie(\nabla_{\mathbf{k}}+\boldsymbol{\Omega})$ [see Eq. (2) in the text] in the $\hat{\mathcal{H}}^{\text{eff}}(\boldsymbol{\kappa},t)$ representation. Assuming that the electrons do not interact with each other (except for obeying Pauli's exclusion principle), one can then write

$$\mathbf{P}(t)=-\frac{ie}{\mathcal{V}}\sum_{s,\mathbf{k}}\sum_{s',s''}f_{s\mathbf{k}}O^{\dagger}_{ss'}(\boldsymbol{\kappa},t)[\delta_{s's''}\nabla_{\mathbf{k}}+\boldsymbol{\Omega}_{s's''}(\boldsymbol{\kappa})]O_{s''s}(\boldsymbol{\kappa},t), \tag{A13}$$

where $f_{s\mathbf{k}}$ is the Fermi-Dirac distribution function over the band states.

As has already been mentioned, the heart of the problem at hand is finding the solution of Eq. (A10) for the matrix of the unitary transformation. It does not seem possible to solve this equation exactly because of its complexity. However, one may try to find an approximate solution in the following formal way. First of all, notice that the $\boldsymbol{\kappa}$, which involves the external field through the vector potential $\mathbf{A}(t)$, enters Eq. (A10) as a parameter. It is clear that the solution of Eq. (A10) does not depend on what the parameter $\boldsymbol{\kappa}$ is. This enables one to put $\boldsymbol{\kappa}=\mathbf{k}$ in Eq. (A10) and, on solving that equation and determining the matrix $O_{ss'}(\mathbf{k},t)$, to obtain $O_{ss'}(\boldsymbol{\kappa},t)$ by substituting $\boldsymbol{\kappa}$ for $\mathbf{k}$ in the expression for $O_{ss'}(\mathbf{k},t)$. The basic idea, thereby, is that for $\boldsymbol{\kappa}=\mathbf{k}$, we can look for a solution of Eq. (A10) iteratively in the form of the perturbation series expansion in powers of the electric field amplitude E

$$\hat{O}(\mathbf{k},t)=\hat{I}+\sum_j\hat{O}_j(\mathbf{k},t), \tag{A14}$$

where $\hat{I}$ is the unit operator and $\hat{O}_j(\mathbf{k},t)$ is of order $j(=1,2,\ldots)$ in the field intensity. We may then expect that the polarization $\mathbf{P}(t)$ can also be expanded in powers of the field

$$\mathbf{P}(t)=\mathbf{P}_0+\sum_j\mathbf{P}_j(t), \tag{A15}$$

where the second ($\mathbf{P}_1$) and the third ($\mathbf{P}_2$) terms in this series correspond to the linear and second-order nonlinear optical responses of the system, respectively. If the external electric field $\mathbf{E}(t)$ is a superposition of two monochromatic waves at frequencies ω_1 and ω_2, the $\alpha(=x,y,z)$ component of the vector $\mathbf{P}_2$ (more precisely, its Fourier transform in time) can be expressed in terms of the second-order NLO susceptibility tensor $\chi^{(2)}_{\alpha\beta\gamma}(-\omega_\sigma;\omega_1,\omega_2)$ as follows:

$$P_{2\alpha}(\omega_\sigma)=\chi^{(2)}_{\alpha\beta\gamma}(-\omega_\sigma;\omega_1,\omega_2)E_\beta(\omega_1)E_\gamma(\omega_2). \tag{A16}$$

Here and hereafter repeated Greek indices and frequencies are assumed to be summed over.

As follows from the above equations, in order to derive an explicit form of $\chi^{(2)}_{\alpha\beta\gamma}(-\omega_\sigma;\omega_1,\omega_2)$, one needs to determine the elements of the matrix $O_{ss'}(\mathbf{k},t)$ up to second order in E. To within the same order, the effective Hamiltonian in Eq. (A12) is given by (for $\boldsymbol{\kappa}=\mathbf{k}$ now)

$$\hat{\mathcal{H}}^{\text{eff}}(\mathbf{k},t)=\hat{\mathcal{H}}^{\text{eff}}_0(\mathbf{k},t)+\hat{\mathcal{H}}^{\text{eff}}_1(\mathbf{k},t)+\hat{\mathcal{H}}^{\text{eff}}_2(\mathbf{k},t), \tag{A17}$$

where

$$\hat{\mathcal{H}}^{\text{eff}}_0(\mathbf{k},t)=\hat{\mathcal{H}}_0(\mathbf{k}), \tag{A18}$$

$$\hat{\mathcal{H}}^{\text{eff}}_1(\mathbf{k},t)=[\hat{\mathcal{H}}_0(\mathbf{k}),\hat{O}_1(\mathbf{k},t)]+\hat{\mathcal{H}}_1(\mathbf{k},t)-i\hbar\frac{\partial}{\partial t}\hat{O}_1(\mathbf{k},t), \tag{A19}$$

$$\hat{\mathcal{H}}^{\text{eff}}_2(\mathbf{k},t)=[\hat{\mathcal{H}}_0(\mathbf{k}),\hat{O}_2(\mathbf{k},t)]+\hat{\mathcal{H}}_1(\mathbf{k},t)\hat{O}_1(\mathbf{k},t) + ie\nabla_{\mathbf{k}}\hat{O}_1(\mathbf{k},t)\mathbf{E}(t)-\hat{O}_1(\mathbf{k},t)\hat{\mathcal{H}}_{1d}(\mathbf{k},t) - i\hbar\frac{\partial}{\partial t}\hat{O}_2(\mathbf{k},t). \tag{A20}$$

Here the square brackets stand for the commutator of the two operators they contain, and the subscript d for the operator $\hat{\mathcal{H}}_1(\mathbf{k},t)$ means that only the diagonal part of the operator should be taken. In deriving Eqs. (A19) and (A20), the following relations for the diagonal and nondiagonal elements of the matrices $O_{1ss'}$ and $O_{2ss'}$ have been used:

$$O_{1ss}(\mathbf{k},t)=O^{\dagger}_{1ss}(\mathbf{k},t)=0, \tag{A21}$$

$$O_{1ss'}(\mathbf{k},t)=-O^{\dagger}_{1ss'}(\mathbf{k},t), \tag{A22}$$

$$O_{2ss}(\mathbf{k},t)=O^{\dagger}_{2ss}(\mathbf{k},t)=\frac{1}{2}\sum_{s'\neq s}O_{1ss'}(\mathbf{k},t)O_{1s's}(\mathbf{k},t), \tag{A23}$$

$$O_{2ss'}(\mathbf{k},t) = -O^{\dagger}_{2ss'}(\mathbf{k},t) - \sum_{s''} O^{\dagger}_{1ss''}(\mathbf{k},t) O_{1s''s'}(\mathbf{k},t). \tag{A24}$$

Note that Eqs. (A22) and (A24) for the nondiagonal elements $O_{1ss'}$ and $O_{2ss'}$, respectively, are obtained by substituting the expansion for the unitary operator $\hat{O}(\mathbf{k},t)$ [Eq. (A14)] in the identity

$$\hat{O}^{\dagger}(\mathbf{k},t)\hat{O}(\mathbf{k},t) = \hat{I}, \tag{A25}$$

and by collecting the terms of one and the same order in E. The relations for the diagonal elements O_{1ss} and O_{2ss} [Eqs. (A21) and (A23), respectively] are obtained similarly provided that those elements can be chosen to be real.

Substituting Eqs. (A18)–(A20) one by one in Eq. (A10) and then solving successively the resulting equations for the elements of the matrices $O_{1ss'}(\mathbf{k},t)$ and $O_{2ss'}(\mathbf{k},t)$, one finds that

$$O_{1ss'}(\mathbf{k},t) = \begin{cases} -\dfrac{ie}{\hbar}\dfrac{\Omega^{\alpha}_{ss'}(\mathbf{k})}{\omega_{ss'}(\mathbf{k}) - \omega} E_{\alpha}(\omega)\exp(-i\omega t) & \text{for } s \neq s', \\ 0 & \text{for } s = s', \end{cases} \tag{A26}$$

$$O_{2ss'}(\mathbf{k},t) = -\frac{e^2}{\hbar^2[\omega_{ss'}(\mathbf{k}) - \omega_{\sigma}]} \left\{ \frac{\partial}{\partial k_{\beta}} \left[\frac{\Omega^{\alpha}_{ss'}(\mathbf{k})}{\omega_{ss'}(\mathbf{k}) - \omega_1} \right] - \frac{\Omega^{\alpha}_{ss'}(\mathbf{k})\Omega^{\beta}_{s's'}(\mathbf{k})}{\omega_{ss'}(\mathbf{k}) - \omega_1} + \sum_{s'' \neq s'} \frac{\Omega^{\beta}_{ss''}(\mathbf{k})\Omega^{\alpha}_{s''s'}(\mathbf{k})}{\omega_{s''s'}(\mathbf{k}) - \omega_1} \right\} \times E_{\alpha}(\omega_1)E_{\beta}(\omega_2)\exp(-i\omega_{\sigma}t) \quad \text{for } s \neq s', \tag{A27}$$

$$O_{2ss}(\mathbf{k},t) = -\frac{e^2}{2\hbar^2} \sum_{s' \neq s} \frac{\Omega^{\alpha}_{ss'}(\mathbf{k})\Omega^{\beta}_{s's}(\mathbf{k})}{[\omega_{ss'}(\mathbf{k}) - \omega_1][\omega_{s's}(\mathbf{k}) - \omega_2]} \times E_{\alpha}(\omega_1)E_{\beta}(\omega_2)\exp(-i\omega_{\sigma}t), \tag{A28}$$

where $\hbar\omega_{ss'}(\mathbf{k})$ is the interband transition energy,

$$\hbar\omega_{ss'}(\mathbf{k}) = \varepsilon_{s\mathbf{k}} - \varepsilon_{s'\mathbf{k}}, \tag{A29}$$

and the superscript $\alpha(\beta)$ for the matrix element $\Omega^{\alpha(\beta)}_{ss'}(\mathbf{k})$ indicates the $\alpha(\beta)$ Cartesian component of the vector $\mathbf{\Omega}_{ss'}(\mathbf{k})$.

Now, having in hand the desired solutions to Eq. (A10) for $\boldsymbol{\kappa}=\mathbf{k}$, we can easily get those in the general case $\boldsymbol{\kappa}\neq\mathbf{k}$, simply replacing $\mathbf{k}$ by $\boldsymbol{\kappa}$ in Eqs. (A26)–(A28). After such a replacement, however, the expansions for $\hat{O}$ and $\mathbf{P}$ in Eqs. (A14) and (A15), respectively, are clearly no longer the expansions in powers of the electric field E. Indeed, each right-hand-side term of Eq. (A15), beginning with the first one, contains E to all orders, due to the dependence of both the $\hat{O}$ and the $\mathbf{\Omega}$, entering Eq. (A13), on $\boldsymbol{\kappa}$. To make sure of this, it is enough to write down the explicit expressions for $\mathbf{P}_0$, $\mathbf{P}_1$, and $\mathbf{P}_2$ in terms of $\hat{O}_j(\boldsymbol{\kappa},t)$ and $\mathbf{\Omega}(\boldsymbol{\kappa})$. It follows from Eq. (A13) that

$$\mathbf{P}_0 = -\frac{ie}{\mathcal{V}} \sum_{s,\mathbf{k}} f_{s\mathbf{k}} \mathbf{\Omega}_{ss}(\boldsymbol{\kappa}), \tag{A30}$$

$$\mathbf{P}_1 = -\frac{ie}{\mathcal{V}} \sum_{s,\mathbf{k}} \sum_{s'} f_{s\mathbf{k}} [O^{\dagger}_{1ss'}(\boldsymbol{\kappa},t)\mathbf{\Omega}_{s's}(\boldsymbol{\kappa}) + \mathbf{\Omega}_{s's}(\boldsymbol{\kappa})O_{1s's}(\boldsymbol{\kappa},t)], \tag{A31}$$

$$\mathbf{P}_2 = -\frac{ie}{\mathcal{V}} \sum_{s,\mathbf{k}} \sum_{s',s''} f_{s\mathbf{k}} \Big\{ [O^{\dagger}_{2ss'}(\boldsymbol{\kappa},t)\mathbf{\Omega}_{s's}(\boldsymbol{\kappa}) + \mathbf{\Omega}_{ss'}(\boldsymbol{\kappa})O_{2s's}(\boldsymbol{\kappa},t)]\delta_{s''s} + O^{\dagger}_{1ss'}(\boldsymbol{\kappa},t)\mathbf{\Omega}_{s's''}(\boldsymbol{\kappa})O_{1s''s}(\boldsymbol{\kappa},t) + \frac{1}{2}[O^{\dagger}_{1ss'}(\boldsymbol{\kappa},t)\nabla_{\mathbf{k}}O_{1s's}(\boldsymbol{\kappa},t) - O^{\dagger}_{1s's}(\boldsymbol{\kappa},t)\nabla_{\mathbf{k}}O^{\dagger}_{1ss'}(\boldsymbol{\kappa},t)]\delta_{s''s'} \Big\}. \tag{A32}$$

Using the above equations, it is easy to show that Eq. (A15) for $\boldsymbol{\kappa}\neq\mathbf{k}$ is actually an expansion of $\mathbf{P}$ in powers of the parameter $\hbar\omega/\Delta$ in the sense that

$$\frac{P_1}{P_0} \approx \frac{P_2}{P_1} \approx \cdots \frac{P_i}{P_{i-1}} \approx \frac{\hbar\omega}{\Delta}, \tag{A33}$$

where Δ is some average energy typical of the interband transitions. This result may be understood by noting that each of the multiplies, standing after $f_{s\mathbf{k}}$ in Eqs. (A30)–(A32), represents a function $\mathcal{F}(\boldsymbol{\kappa})$ of the variable $\boldsymbol{\kappa}=\mathbf{k}+(e/\hbar c)\mathbf{A}$, which is regular in the neighborhood of the point $\boldsymbol{\kappa}=\mathbf{k}$ and can therefore be represented there by its Taylor series. Assuming that the characteristic scale in which the function $\mathcal{F}(\mathbf{k})$ varies substantially is determined by the lattice constant a_0, we may estimate the derivatives entering Taylor's expansion for the function $\mathcal{F}(\boldsymbol{\kappa})$ by setting

$$\mathcal{F}'(\boldsymbol{\kappa}=\mathbf{k}) \sim \frac{\mathcal{F}(\mathbf{k})}{k} \sim a_0\mathcal{F}(\mathbf{k}),$$

$$\mathcal{F}''(\boldsymbol{\kappa}=\mathbf{k}) \sim \frac{\mathcal{F}(\mathbf{k})}{k^2} \sim a_0^2\mathcal{F}(\mathbf{k}), \tag{A34}$$

and so on, where the prime denotes differentiation with respect to κ. In such a heuristic way, we arrive at the following expansion for $\mathcal{F}(\boldsymbol{\kappa})$ in terms of $\mathcal{F}(\mathbf{k})$ and E:

$$\mathcal{F}(\boldsymbol{\kappa}) \approx \mathcal{F}(\mathbf{k}) \sum_{n=0}^{\infty} \frac{\xi_E^n}{n!}, \tag{A35}$$

where

$$\xi_E = \frac{eEa_0}{\hbar\omega}, \tag{A36}$$

and $\mathcal{F}(\mathbf{k})$ is the abbreviated uniform notation for the multipliers standing after $f_{s\mathbf{k}}$ in Eqs. (A30)–(A32) where $\boldsymbol{\kappa}$ replaced by $\mathbf{k}$. It is clear, therefore, that Eq. (A35) is gener-

ally not an expansion in powers of the electric field: the multipliers in Eqs. (A31) and (A32), by themselves, depend on E even when $\boldsymbol{\kappa}=\mathbf{k}$ [see Eqs. (A26)–(A28)]. Turning back to the last equations in conjunction with Eq. (A14), it is seen that the expansion in Eq. (A14) is actually developing in powers of the parameter

$$\eta_E = \frac{eEa_0}{\Delta} = \frac{\hbar\omega}{\Delta}\xi_E, \tag{A37}$$

if we assume that $\Omega^{\alpha}_{ss'}(\mathbf{k})$ is on the order of a_0. Based on this observation, and using Eq. (A35) in Eqs. (A30)–(A32), we arrive at the result stated in Eq. (A33).

From the above discussion, we can conclude that it will be justified to write $\mathbf{P}_2$ as defined in Eq. (A32), but with $\boldsymbol{\kappa}$ replaced by $\mathbf{k}$, if we are concerned with the range of the external field strength E in which the parameters ξ_E and η_E are both small as compared to 1 (it is clearly not necessary for the parameter $\hbar\omega/\Delta$ to be small either). This is consistent with the conventional phenomenological definition of $\mathbf{P}_2$ in terms of the $\chi^{(2)}$-susceptibility tensor components, which is given by Eq. (A16) in our notation. The same conclusion holds true for $\mathbf{P}_1$ defined in Eq. (A31) as well.

In principle, Eq. (A32) enables us to calculate the second-order dipole-moment density $\mathbf{P}_2$ induced by the incident radiation fields with arbitrary polarizations. However, in what follows, we confine ourselves to the experimental situation, which we are interested in the text, where all the fundamental fields are polarized in the same direction which is chosen to be the z direction. In this case, it is enough to consider the component $\chi^{(2)}_{zzz}(-\omega_\sigma;\omega_1,\omega_2)$ of the susceptibility tensor defined in Eq. (A16), which we denote simply $\chi^{(2)}(-\omega_\sigma;\omega_1,\omega_2)$ in the text. Taking into account that the tensor is invariant under all $(2+1)!$ permutations of the frequencies ω_1, ω_2, $-\omega_\sigma$ (Ref. 22) and using Eqs. (A21)–(A24) together with Eqs. (A26)–(A28), we finally obtain

$$\chi^{(2)}(-\omega_\sigma;\omega_1,\omega_2) = \chi^{(2)}_{\mathrm{I}}(-\omega_\sigma;\omega_1,\omega_2) + \chi^{(2)}_{\mathrm{II}}(-\omega_\sigma;\omega_1,\omega_2) + \chi^{(2)}_{\mathrm{III}}(-\omega_\sigma;\omega_1,\omega_2), \tag{A38}$$

where

$$\chi^{(2)}_{\mathrm{I}}(-\omega_\sigma;\omega_1,\omega_2) = \frac{ie^3}{2\mathcal{V}\hbar^2}\sum_{s,\mathbf{k}}\sum_{s'\neq s}\sum_{P} f_{s\mathbf{k}} \times \frac{\Omega_{ss'}(\mathbf{k})[\Omega_{ss}(\mathbf{k})-\Omega_{s's'}(\mathbf{k})]\Omega_{s's}(\mathbf{k})}{[\omega_{ss'}(\mathbf{k})-\omega_1][\omega_{s's}(\mathbf{k})-\omega_2]}, \tag{A39}$$

$$\chi^{(2)}_{\mathrm{II}}(-\omega_\sigma;\omega_1,\omega_2) = \frac{ie^3}{4\mathcal{V}\hbar^2}\sum_{s,\mathbf{k}}\sum_{s'\neq s}\sum_{P} f_{s\mathbf{k}} \times \left\{ \frac{\Omega_{s's}(\mathbf{k})}{\omega_{s's}(\mathbf{k})-\omega_1}\frac{\partial}{\partial k}\left[\frac{\Omega_{ss'}(\mathbf{k})}{\omega_{ss'}(\mathbf{k})-\omega_2}\right] - \frac{\Omega_{ss'}(\mathbf{k})}{\omega_{ss'}(\mathbf{k})-\omega_1}\frac{\partial}{\partial k}\left[\frac{\Omega_{s's}(\mathbf{k})}{\omega_{s's}(\mathbf{k})-\omega_2}\right]\right\}, \tag{A40}$$

$$\chi^{(2)}_{\mathrm{III}}(-\omega_\sigma;\omega_1,\omega_2) = \frac{ie^3}{6\mathcal{V}\hbar^2}\sum_{s,\mathbf{k}}\sum_{s'\neq s}\sum_{s''\neq s,s'}\sum_{P} f_{s\mathbf{k}} \times \left\{ \frac{\Omega_{ss'}(\mathbf{k})\Omega_{s's''}(\mathbf{k})\Omega_{s''s}(\mathbf{k})}{[\omega_{s's''}(\mathbf{k})-\omega_1][\omega_{s''s}(\mathbf{k})-\omega_2]} + \frac{\Omega_{ss''}(\mathbf{k})\Omega_{s''s'}(\mathbf{k})\Omega_{s's}(\mathbf{k})}{[\omega_{ss''}(\mathbf{k})-\omega_1][\omega_{s''s'}(\mathbf{k})-\omega_2]}\right\}. \tag{A41}$$

Here, as before in the text, Σ_P denotes the sum over all permutations of frequencies ω_1, ω_2, $-\omega_\sigma$, and $\Omega^{z}_{ss'}(\mathbf{k})$ and $\partial/\partial k_z$ are abbreviated as $\Omega_{ss'}(\mathbf{k})$ and $\partial/\partial k$, respectively.

For a system with an arbitrary number of bands, the above expression for $\chi^{(2)}(-\omega_\sigma;\omega_1,\omega_2)$ is very complicated, involving various two-band contributions [the first and the second terms in Eq. (A38)] as well as three-band ones [the last term in Eq. (A38)]. In the present paper we are interested in the NLO properties of undoped BN-SWNTs with an effectively two-band π-electronic structure. For such a system, the term $\chi^{(2)}_{\mathrm{III}}$ vanishes identically and, treating the $\chi^{(2)}_{\mathrm{I}}$ and the $\chi^{(2)}_{\mathrm{II}}$ terms at absolute zero temperature, we get the results stated in Eqs. (4) and (5) in the text.

*612033@inbox.ru

[1] A. Rubio, J. L. Corkill, and M. L. Cohen, Phys. Rev. B **49**, 5081 (1994).

[2] X. Blase, A. Rubio, S. G. Louie, and M. L. Cohen, Europhys. Lett. **28**, 335 (1994).

[3] L. Boulanger, B. Andriot, M. Cauchetier, and F. Willaime, Chem. Phys. Lett. **234**, 227 (1995).

[4] N. G. Chopra, R. J. Luyken, K. Cherrey, V. H. Crespi, M. L. Cohen, S. G. Louie, and A. Zettl, Science **269**, 966 (1995).

[5] M. Terrones, J. M. Romo-Herrera, E. Cruz-Silva, F. López-Urias, E. Muñoz-Sandoval, J. J. Velázquez-Salazar, H. Terrones, Y. Bando, and D. Golberg, Mater. Today **10**, 30 (2007).

[6] R. Saito, G. Dresselhaus, and M. S. Dresselhaus, *Physical Properties of Carbon Nanotubes* (Imperial College Press, London, 1998).

[7] W. Q. Han, W. Michalson, J. Cummings, and A. Zettl, Appl. Phys. Lett. **81**, 1110 (2002).

[8] Y. Chen, J. Zou, S. J. Campbel, and G. L. Caer, Appl. Phys. Lett. **84**, 2430 (2004).

[9] G. Y. Guo and J. C. Lin, Phys. Rev. B **72**, 075416 (2005); **77**, 049901(E) (2008).

[10] O. E. Alon, Phys. Rev. B **64**, 153408 (2001).

[11] Vl. A. Margulis, E. E. Muryumin, and E. A. Gaiduk, Phys. Rev. B **77**, 035425 (2008).

[12] V. M. Genkin and P. M. Mednis, Zh. Eksp. Teor. Fiz. **54**, 1137 (1968) [Sov. Phys. JETP **27**, 609 (1968)]; Fiz. Tverd. Tela (Leningrad) **10**, 3 (1968) [Sov. Phys. Solid State **10**, 1 (1968)].
[13] E. Ghahramani, D. J. Moss, and J. E. Sipe, Phys. Rev. Lett. **64**, 2815 (1990); Phys. Rev. B **43**, 8990 (1991).
[14] M. Terauchi, M. Tanaka, K. Suzuki, A. Ogino, and K. Kimura, Chem. Phys. Lett. **324**, 359 (2000).
[15] R. S. Lee, J. Gavillet, M. Lamy de la Chapelle, A. Loiseau, J.-L. Cochon, D. Pigache, J. Thibault, and F. Willaime, Phys. Rev. B **64**, 121405(R) (2001).
[16] J. Wang, V. K. Kayastha, Y. K. Yap, Z. Fan, J. G. Lu, Z. Pan, I. N. Ivanov, A. A. Puretzky, and D. B. Geohegan, Nano Lett. **5**, 2528 (2005).
[17] Vl. A. Margulis, E. A. Gaiduk, E. E. Muryumin, O. V. Boyarkina, and L. V. Fomina, Phys. Rev. B **74**, 245419 (2006).
[18] H. Ajiki and T. Ando, Physica B **201**, 349 (1994).
[19] N. Bloembergen, *Nonlinear Optics* (Benjamin, New York, 1965), Chap. 2.
[20] J. A. Armstrong, N. Bloembergen, J. Ducuing, and P. S. Pershan, Phys. Rev. **127**, 1918 (1962).
[21] N. Bloembergen and Y. R. Shen, Phys. Rev. **133**, A37 (1964).
[22] P. N. Butcher and T. P. McLean, Proc. Phys. Soc. London **81**, 219 (1963); **83**, 579 (1964).
[23] D. E. Aspnes, Phys. Rev. B **6**, 4648 (1972).
[24] J. E. Sipe and E. Ghahramani, Phys. Rev. B **48**, 11705 (1993).
[25] A. G. Marinopoulos, L. Wirtz, A. Marini, V. Olevano, A. Rubio, and L. Reining, Appl. Phys. A: Mater. Sci. Process. **78**, 1157 (2004).
[26] G. Y. Guo and J. C. Lin, Phys. Rev. B **71**, 165402 (2005).
[27] L. Wirtz, A. Marini, and A. Rubio, Phys. Rev. Lett. **96**, 126104 (2006).
[28] C.-H. Park, C. D. Spataru, and S. G. Louie, Phys. Rev. Lett. **96**, 126105 (2006).
[29] E. M. Lifshitz and L. P. Pitaevskii, *Statistical Physics, Part 2* (Pergamon, New York, 1980), Chap. 6.
[30] E. I. Blount, in *Solid State Physics, Advances in Research and Applications*, edited by F. Seitz and D. Turnbull (Academic, New York, 1962), Vol. 13, p. 305.
[31] P. Král, E. J. Mele, and D. Tománek, Phys. Rev. Lett. **85**, 1512 (2000).
[32] E. J. Mele and P. Král, Phys. Rev. Lett. **88**, 056803 (2002).
[33] S. M. Nakhmanson, A. Calzolari, V. Meunier, J. Bernholc, and M. Buongiorno Nardelli, Phys. Rev. B **67**, 235406 (2003).
[34] C. Aversa and J. E. Sipe, Phys. Rev. B **52**, 14636 (1995).
[35] L. D. Landau, E. M. Lifshitz, and L. P. Pitaevskii, *Electrodynamics of Continuous Media*, 2nd ed. (Pergamon, Oxford, 1984), Chap. 13, Sec. 108.
[36] Vl. A. Margulis, E. E. Muryumin, and E. A. Gaiduk (unpublished).
[37] R. C. Miller, Appl. Phys. Lett. **5**, 17 (1964).
[38] Q. Wu, Z. Hu, X. Wang, Y. Lu, X. Chen, H. Xu, and Y. Chen, J. Am. Chem. Soc. **125**, 10176 (2003).
[39] J. Goldberger, R. He, Y. Zhang, S. Lee, H. Yan, H. Choi, and P. Yang, Nature (London) **422**, 599 (2003).
[40] J. S. Lauret, R. Arenal, F. Ducastelle, A. Loiseau, M. Cau, B. Attal-Tretout, and E. Rosencher, Phys. Rev. Lett. **94**, 037405 (2005).
[41] Note that in our previous paper (Ref. 11) the values of m equal to 9, 10, 11, 12, 13, and 14 have erroneously been attributed (in sequential order) to the first six energy subbands (counted from the Fermi level) of the c and v bands. This error, however, did not affect the results or the conclusions of that paper, which are all correct, except for Eq. (20). The correct form of that equation is presented in this paper [see Eq. (36) in the text].
[42] It is for this reason that the quantity 2Δ is used to normalized the photon energy $\hbar\omega$ throughout the paper.
[43] V. I. Gavrilenko and R. Q. Wu, Phys. Rev. B **61**, 2632 (2000).
[44] Vl. A. Margulis, J. Phys.: Condens. Matter **11**, 3065 (1999); Vl. A. Margulis and T. A. Sizikova, Physica B **245**, 173 (1998); Vl. A. Margulis and E. A. Gaiduk, J. Opt. A, Pure Appl. Opt. **3**, 267 (2001); Vl. A. Margulis, O. V. Boyarkina, and E. A. Gaiduk, Opt. Commun. **249**, 339 (2005).
[45] S. Tatsuura, M. Furuki, Y. Sato, I. Iwasa, M. Tian, and H. Mitsu, Adv. Mater. **15**, 534 (2003); L. Huang, H. N. Pedrosa, and T. D. Krauss, Phys. Rev. Lett. **93**, 017403 (2004); A. Maeda, S. Matsumoto, H. Kishida, T. Takenobu, Y. Iwasa, M. Shiraishi, M. Ata, and H. Okamoto, *ibid.* **94**, 047404 (2005); M. Kamaraju, S. Kumar, A. K. Sood, S. Guha, S. Krishnamurthy, and C. N. R. Rao, Appl. Phys. Lett. **91**, 251103 (2007); D. Shimamoto, T. Sakurai, M. Itoh, Y. A. Kim, T. Hayashi, M. Endo, and M. Terrones, *ibid.* **92**, 081902 (2008).
[46] M. Bass, P. A. Franken, J. F. Ward, and G. Weinreich, Phys. Rev. Lett. **9**, 446 (1962).
[47] J. F. Ward, Phys. Rev. **143**, 569 (1966).
[48] Y. R. Shen, *The Principles of Nonlinear Optics* (Wiley, New York, 1984), Chap. 5, Sec. 5.1.
[49] K. D. Singer, S. L. Lalama, J. E. Sohn, and R. D. Small, in *Nonlinear Optical Properties of Organic Molecules and Crystals*, edited by D. S. Chemla and J. Zyss (Academic, Orlando, 1987), Vol. 1, Chap. 9.
[50] Note that both these values of the electric field E_0 are substantially smaller than its threshold value ($\sim 10^4$ kV/cm) beyond which electron field emission may occur [see K. H. Khoo, M. S. C. Mazzoni, and S. G. Louie, Phys. Rev. B **69**, 201401(R) (2004)].
[51] E. Rosencher and Ph. Bois, Phys. Rev. B **44**, 11315 (1991).